

Hydrogen reactions with dopants and impurities in solar silicon from first principles

José Coutinho¹,¹ Diana Gomes¹,¹ Vitor J. B. Torres¹,¹ Tarek O. Abdul Fattah²,² Vladimir P. Markevich²,² and Anthony R. Peaker²

¹*i3N and Department of Physics, University of Aveiro, Campus Santiago, 3810-193 Aveiro, Portugal**

²*Photon Science Institute and Department of Electrical and Electronic Engineering, The University of Manchester, Manchester M13 9PL, United Kingdom*

We present a theoretical account of some of the most likely hydrogen-related reactions with impurities in n-type and p-type solar-grade silicon. These include reactions with dopants and carbon, which are relevant in the context of life-time degradation of silicon solar cells, most notably of light and elevated temperature degradation (LeTID) of the cells. Among the problems addressed, we highlight a comparative study of acceptor-enhanced dissociation of hydrogen molecules in B- and Ga-doped material, their subsequent reaction steps toward formation of acceptor-hydrogen pairs, the proposal of mechanisms which explain the observed kinetics of photo-/carrier-induced dissociation of PH and CH pairs in n-type Si, analysis of reactions involving direct interactions between molecules with P and C, and the assignment of several electron and hole traps with detailed atomistic- and wavefunction-resolved models.

Pre-print published in Solar RRL 8, 2300639 (2024)

DOI:10.1002/solr.202300639

I. INTRODUCTION

Over the last two decades, a combination of cost reduction with improvement in material quality, changed the list of concerns regarding the various sources of bulk life-time degradation of solar silicon. For instance, while transition metal contamination became avoidable, the boron-oxygen light induced degradation gained relevance [1–3], justifying a first push toward replacing boron (a long-standing dopant of choice), by alternative dopants [4–8]. According to the International Technology Roadmap for Photovoltaic [9], Ga-doped p-type Cz-Si already dominates the market share in 2023, and will remain the dominant material within the next 10 years.

A second and more recent reason for exploring alternative dopants other than boron, has been Light- and elevated-Temperature-Induced Degradation (LeTID) of solar Si [10, 11]. This is a crucially important degradation mechanism, as modules show a substantial decrease of conversion efficiency (up to 16% relative) during their operating life. It is now recognized that LeTID can affect cells made of different Si materials, including p- and n-type [12–15], although it is not clear if the source of the problem is the same in all cases.

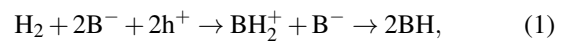
While degradation in the field takes years to manifest, LeTID can be accelerated by increasing the operating temperature to ~ 70 - 100 °C with illumination of ~ 1 sun (1 kW/m^2), or more usually in lab tests by passing a current to inject minority carriers equivalent to the population produced during normal operation. This is sometimes referred to as carrier induced degradation (CID), and produces very similar results to illumination. Many variants of accelerated LeTID/CID appear in the literature ranging from high intensity laser irradiation to dark annealing. It seems nevertheless that degradation and recovery take place simultaneously at different rates with thermal activation energies close to 1 eV [16]. This may go some way to explain the differences in observed be-

havior, but in an attempt to standardize rapid LeTID testing, procedures for commercial applications have been drawn up *e.g.* SEMI PV93 and IEC 61215. These testing methods also include methodologies that minimize interference from iron-related and boron-oxygen light induced degradation effects.

Importantly, there is a very substantial literature on LeTID which relates the magnitude of the effect to the fast-firing step in the fabrication process. Although there are wide variations in the results, it now seems certain that hydrogen is implicated (see for instance Refs. [16, 17] and references therein).

Molecular hydrogen is well known to form upon quenching p-type and n-type Si in contact with a hydrogen source at high temperature [18–20]. The molecules constitute the main stock of hydrogen in the Si of *as-fired* solar cells, and originates from the hydrogen-rich passivating oxide/nitride stack [21]. In pristine Si they become mobile just above room temperature. However, in O-rich material they are lightly bound to interstitial oxygen atoms and one needs to raise the temperature over 70 °C to initiate molecular motion [22], and possibly, to induce LeTID.

Several models for LeTID have been hypothesized, but as yet, a detailed mechanism or mechanisms remain unclear. We recently proposed that a possible culprit for the non-radiative recombination activity behind LeTID in boron-doped Si is a complex made of boron and two hydrogen atoms [23]. Accordingly, BH_2 is a byproduct of the reaction between a non-equilibrium population of H_2 molecules with boron, when the molecules become mobile above room temperature. From first-principles calculations, we found that the first and second steps toward the right of the reaction,



were limited by activation barriers of 1.1 eV and 0.8 eV [24]. These are considerably lower than the barrier for H_2 dissociation in pristine Si (1.6 eV [25]), and hence boron was claimed to act as a catalyst for the breaking of H_2 , and facilitate BH pair formation.

* jose.coutinho@ua.pt

The calculated value of the energy barrier for the first reaction in sequence 1 accounts well for the activation energy of the degradation stage of 1.08 eV determined for B-doped multi crystalline Si [26]. It is also in line with recent findings which show that LeTID develops concurrently with the early stages of BH formation [27, 28].

It has been argued in Ref. [29] that GaH₂ complexes are effective-mass-like shallow donors, and unlike BH₂, they should not act as recombination centers. It is therefore hard to understand how a GaH₂ analogue of the BH₂ complex could explain the observation of LeTID in cells made from Ga-doped substrates [15, 30, 31]. Similar arguments apply to the degradation observed in n-type based cells (although in this case the effect is weaker and slower) [13, 17, 32]. Possibilities could involve contamination of the materials with boron, or alternatively that H₂ dissociation is just the first step for the formation of a mix of different hydrogen-related electrically active centers (among which we have BH₂).

Presently, passivated emitter and rear cell (PERC) architecture dominates the photovoltaic market [33]. Front and back passivation layers make these devices particularly vulnerable to LeTID. Solar cells using new concepts like n-type based tunneling oxide passivated contacts (TOPCon) and silicon heterojunction (SHJ) cells, although show improved lifetime stability, also seem to be affected by LeTID [5].

It is therefore of uttermost importance to understand the reactions involving hydrogen in n-type Si, including the effect of minority carriers, and ideally using state-of-the-art quantum mechanical calculations. We cannot provide an extensive review of previous work on hydrogen in Si. For that we direct the reader for instance to Refs. [25, 34, 35] and references therein. It is however useful to summarize some properties which are especially relevant in the present context.

Atomic H in Si is an amphoteric element — it is an acceptor and a donor in n-type and p-type Si, respectively [36–38]. H⁺ sits at the center of a Si-Si bond, while H⁻ occupies a tetrahedral interstitial cage [39, 40]. The neutral state is metastable and disproportionates into ionic species, H⁰ → xH⁺ + (1 - x)H⁻, with x depending on the Fermi level with respect to the negative-U (-/+) transition [40, 41]. Isolated hydrogen is very reactive and mobile, making it virtually inexistent under equilibrium conditions at room temperature. However, it can show up transiently upon changes of thermodynamic or excitation conditions (e.g. release of H from H-related complexes upon capture of photogenerated carriers). The fractional populations of charge states of free H as a function of temperature has been described by Sun *et al.* [42, 43] using a *general occupancy ratio* model, which incorporates not only information regarding the transition levels of the defects, but also their capture cross sections for free carriers.

Due to its high mobility (the diffusion length of H⁺ is about 1.4 μm at room temperature [44]), hydrogen interacts with other available lattice defects, most effectively with defects which have an opposite charge [36, 44, 45]. The problem of diffusivity of H atoms in differently doped Si crystals has been considered recently in Ref. [25]. Reactions between hydrogen and group-III elements in Si were also addressed theoretically using hybrid density functional theory [24]. However, a com-

parable study of interactions between hydrogen and group-V elements is not available, and as far as we are aware, there are no reports either demonstrating or ruling out the existence of direct interactions between H₂ and donors in Si. A clarification of this issue would be welcome in the context of solar Si.

Hydrogen passivation of group-V donors in Si is a well documented topic [46–52]. Phosphorus-H defects show a ≡P Si-H_{AB} geometry, where the H atom binds to Si, oppositely to a broken P-Si bond, leaving the P atom three-fold coordinated [48, 49, 53]. This location is commonly referred to as *anti-bonding* (AB) site, and contrasts with the *bond-center* (BC) site found for the acceptor-H pairs.

Donor-H complexes anneal out around $T \sim 80$ -100 °C, among which PH is the most stable, with dissociation barriers estimated in the range 1.1-1.2 eV [50, 54]. Importantly, in the presence of minority carriers, donor-H pairs become unstable, even below room temperature [55–57]. The effect has been explained by two alternative views: a *dissociative model* [58], where thermal fluctuations promote partial dissociation of PH into close P⁺-H⁻ pairs, enabling hole capture by hydrogen, and subsequent escape of H⁰ or H⁺ from the Coulomb field of the donor. After that, and in the absence of minority carriers (zero bias and darkness), the measured recovery kinetics of resistivity has an activation barrier of 0.7 eV, interpreted as the upper limit for the migration energy of H⁻ before reformation of the pairs [37, 58].

The other view follows a *transformative model* [59, 60], where upon hole capture the ≡P Si-H_{AB} ground state quickly converts into a more stable positively charged ≡P⁺ H_{BC}-Si state, where H jumps into the center of the P-Si bond. The observed 0.7 eV barrier of the passivation recovery kinetics measured in Ref. [58], is in this case attributed to the activation energy of the reverse jump of H, from BC to the AB site in the neutral state after electron capture. However, this picture is only possible if PH has a donor state, a property that has never been demonstrated (nor refuted) experimentally or theoretically.

Other omnipresent impurities in solar Si are carbon and oxygen. The available experimental and theoretical results indicate that OH pairs are weakly-bound and not stable at room temperature [36, 38, 61–64], and therefore are not addressed here. Oxygen-H₂ pairs are not electrically active, and their relevance (especially within the context of LeTID) seems to be that of stabilizing the molecules, *i.e.*, hindering molecular motion at room temperature [22].

Carbon, on the other hand, is able to form stable and electrically active centers upon capture of hydrogen atoms. This paper extends our understanding regarding the formation and properties of CH_n complexes. We focus on reactions involving substitutional carbon and hydrogen under typical conditions of solar cell fabrication and operation. In this case, already known defects are the CH pair and CH₂ complex. The latter, also referred to as CH₂^{*} [65–68], is stable up to about 250 °C and it is electrically inert.

Regarding the CH pair, the picture is not so consensual. According to combined first-principles calculations and Laplace deep level transient spectroscopy (Laplace-DLTS) [69], the

most stable CH defect displays a $\equiv \text{C-H}_{\text{BC}} \text{Si} \equiv$ geometry (possessing an unsaturated Si radical). The defect was connected to donor and acceptor transitions respectively at $E_{\text{v}}+0.33$ eV and $E_{\text{c}} - 0.16$ eV, and in n-type Si it is stable up to just above room temperature in darkness [69]. However, it rapidly disappears under above-band-gap illumination [70]. In p-type Si the CH pair is more stable and anneals out just above 100 °C [71]. The above effects could be important in the context of light-induced reactions in solar silicon, but the mechanisms remain unexplored theoretically.

The above picture for the CH complex, including the structure, location of transition levels, as well as the number of charge states, are also under dispute. Recent capacitance and depth profile measurements led to an alternative view, where several CH complexes could form in wet-etched and plasma-treated material. While there is an agreement regarding the origin of the $E_{\text{c}} - 0.16$ eV acceptor transition (the $\equiv \text{C-H}_{\text{BC}} \text{Si} \equiv$ defect), the $E_{\text{v}}+0.33$ eV level was assigned to an acceptor transition of a C-H complex with a different geometry. Additionally, first and second acceptor levels at $E_{\text{c}} - 0.51$ eV and $E_{\text{c}} - 0.06$ eV were assigned to a $\text{H}_{\text{AB}}\text{-C Si} \equiv$ defect, and a complex with more than one H atom was assigned to an electron trap at $E_{\text{c}} - 0.14$ eV [72]. In that respect, we hope to contribute to the clarification of the matter, especially considering that some of these centers may form transiently, during the relocation of H upon heating or illumination, and possibly lower the minority carrier lifetime in both p-type and n-type Si.

The paper is organized as follows: Section II describes a comparative study of hydrogen reactions (atomic and molecular) with boron and gallium acceptors in p-type Si. In Secs. III and IV we investigate analogous reactions with phosphorus (n-type Si), with emphasis on the minority-carrier-enhanced dissociation of PH. In Secs. V and VI we revisit and extend previous calculations of CH_n complexes with $n \leq 3$. Finally, we lay our conclusions in Sec. VII.

II. DISSOCIATION OF MOLECULAR HYDROGEN UPON REACTION WITH ACCEPTORS

H_2 molecules occupy tetrahedral interstitial cages of the Si lattice. Inspection of the band structure of a supercell with the molecule indicates that it has a clean band gap, *i.e.* cannot trap carriers, irrespectively of its orientation and location within the accessible volume. A fully occupied Kohn-Sham state in the lower half of the gap, which could lead to carrier trapping, appears only after partial dissociation of the molecule into a $\text{H}_{\text{BC}}^+ \text{-H}_{\text{AB}}^-$ pair. This state is achieved upon collision of the molecule with a Si-Si bond, after surmounting an energy barrier of 1.6 eV, and that figure was assigned to the dissociation barrier of isolated H_2 [25].

More recently, we have argued that boron can act as a catalyst for H_2 dissociation by lowering the above barrier to 1.1 eV [24]. The mechanism involves H_2 hitting a Si-B bond and subsequent formation of a metastable state comprising H^- next to a BH pair (BH-H^-). Several processes were hypothesized to follow (including hole capture by the hydride anion), but im-

portantly, the $\text{H}_2 + \text{B}^- \rightarrow \text{BH-H}^-$ step was deemed critical for triggering LeTID in B-doped Si.

Given the controversial results on LeTID in cells based on Ga-doped Si, we have performed a comparative study of H-reactions with B and Ga in Si. Some results already reported include the binding and dissociation energies of BH and GaH pairs. The binding energy was found from the reaction energy $E_{\text{b}} = \Delta E_{\text{R}} = E_{\text{fs}} - E_{\text{is}}$ across $\text{XH} \rightarrow \text{X}^- + \text{H}^+$ (with $\text{X} = \{\text{B, Ga}\}$), where E_{is} and E_{fs} stand for the energy of initial (reactants) and final (products) states, respectively. The dissociation energy of a defect complex is the overall barrier that the system must surmount, starting from its ground state, and reach the dissociated state (uncorrelated constituents, for instance infinitely separated B^- and H^+). This is obtained from the activation energy $E_{\text{d}} = \Delta E_{\text{A}} = E_{\text{ts}} - E_{\text{is}}$ of the above reaction, where E_{ts} is the energy of the transition state, all along the minimum-energy path between reactants and products evaluated using the NEB method.

In principle, the dissociation mechanism involves an infinite sequence of H^+ jumps away from B^- . To make the problem tractable, we calculated the barriers of H^+ jumps from first and second neighboring sites (with respect to the B^- ion), and from sites where H^+ is infinitely separated from B^- . First and second jumps of H away from B and Ga have transition-state energies that are clearly below that of saddle point of H^+ migration at a remote location from B^- [24, 29]. Assuming that the energy barriers of H^+ jumps from sites farther than third neighbors (from X^-) are identical to that of isolated H^+ (calculated as $E_{\text{m}} = 0.42$ eV), we conclude that the dissociation energy of the pairs is $E_{\text{d}} = E_{\text{b}} + E_{\text{m}}$.

The results are shown in Table I (the boron-related data is reproduced from Ref. [24]). For BH, the calculated binding and dissociation energies are $E_{\text{b}} = 0.76$ eV and $E_{\text{d}} = E_{\text{b}} + E_{\text{m}} = 1.18$ eV. They are relatively lower than the $E_{\text{b}} = 0.92$ eV and $E_{\text{d}} = 1.34$ eV analogues for GaH. These results agree well with those derived from capacitance-voltage measurements by Zundel and Weber [73], who reported $E_{\text{d}} = 1.28$ eV and 1.40 eV for BH and GaH, respectively.

The comparison between experimental and calculated activation energies of defect reactions should be done with care. Usually, several defect reactions, including interactions with carriers, take place in parallel during experiments designed to follow the loss or growth of a specific complex. For instance, reliable values of dissociation energies of XH pairs, free of some back-reaction effects, could only be measured in the depletion region of reverse-biased diodes [73]. The excellent agreement between those results and our calculations is reassuring regarding the interpretation of the data.

From a comprehensive exploration of the potential energy surface involving the motion of H^+ next to B^- and Ga^- we could arrive at the reaction and dissociation energies reported in the topmost three rows of Table I [24, 29]. Disproportionation of two XH defects into XH_2^+ and X^- (second row) is endothermic, and therefore XH_2^+ is metastable with respect to XH formation. Along such H^+ exchange reaction, the total energy is always lower than that of the intermediate $\text{XH} + \text{X}^- + \text{H}^+$ state plus the migration barrier of H^+ . Hence,

Table I. Calculated reaction and activation energies (ΔE_R and ΔE_A , respectively) for formation of acceptor-hydrogen complexes in p-type silicon. $\Delta E_R = E_{fs} - E_{is}$ and $\Delta E_A = E_{is} - E_{is}$, where subscripts ‘is’, ‘ts’ and ‘fs’ stand for initial, transition and final states of the reaction on the leftmost column, respectively. All values are in eV.

Acceptor (X) Reaction	Boron		Gallium	
	ΔE_R	ΔE_A	ΔE_R	ΔE_A
$X^- + H^+ \rightarrow XH$	-0.76	0.42	-0.92	0.42
$2XH \rightarrow X^- + XH_2^+$	+0.36	1.18	+0.43	1.34
$XH + H^+ \rightarrow XH_2^+$	-0.40	0.42	-0.48	0.42
$H_2 + X^- \rightarrow XH_2^-$	-0.31	1.1	+0.14	1.4
$H_2 + X^- + 2h^+ \rightarrow XH_2^+$	-0.83	1.10	-1.07	1.05
$H_2 + 2X^- + 2h^+ \rightarrow 2XH$	-1.19	1.10	-1.50	1.05

the activation energy for $2XH \rightarrow X^- + XH_2^+$ corresponds to the dissociation barrier of XH.

Despite being metastable with respect to XH formation, XH_2^+ complexes can form upon capture of H^+ by XH pairs in the presence of large concentrations of atomic hydrogen [23, 29]. The reaction (third row of Table I) is energetically favorable ($\Delta E_R = -0.40$ eV and -0.48 eV for $X = B$ and Ga, respectively). The very last barrier before formation of XH_2^+ , which involves a jump of H^+ into the center of a X-Si bond of the XH pair ($XH-H^+ \rightarrow XH_2^+$), was calculated as 0.46 eV and 0.36 eV for $X = B$ and Ga, respectively. Hence, formation of XH_2^+ via capture of H^+ by XH in X-doped Si is anticipated to show an activation energy similar to the migration barrier of H^+ .

While the reaction mechanism between H_2 and B^- has been addressed already, the analogous process involving H_2 and Ga^- is uncharted. In Ref. [24] we found that formation of a metastable ($BH-H^-$) state precedes subsequent reactions toward formation of BH_2^+ . Figure 1(a) generalizes the mechanism for either $X = B$ and Ga, presenting two possible routes for attaining XH_2^+ via formation of metastable $XH-H^-$. Hole capture should be involved in both routes. The release of protons (not shown) with corresponding formation of additional XH pairs is also possible.

In step 1 ($H_2 + X^- \rightarrow XH-H^-$), the molecule strikes the X-Si bond and that has an energy barrier of 1.10 eV and 1.05 eV for $X = B$ and Ga, respectively. The $XH-H^-$ landing state is 0.59 and 0.89 eV above the $H_2 + X^-$ initial state for $X = B$ and Ga, respectively. Its atomistic geometry is shown in Figure 1(b) for the case of $GaH-H^-$, where an interstitial H^- hydride sits next to a neutral GaH pair.

Activation energies for jumps of H^- in both $BH-H^-$ and $GaH-H^-$ into a neighboring interstitial cage was estimated about 0.5 eV. If we add this figure to the energy of the $XH-H^-$ state we find 1.1 eV and 1.4 eV for the barrier that has to be surmounted to reach the XH_2^- (A) acceptor state (steps 1 and 2a combined) for $X = B$ and Ga, respectively. The label ‘A’ emphasizes that the complex is an *acceptor* and adopts an axial ($Si-H_{BC} X-H_{AB}$) geometry, where both Si and X are four-fold coordinated. The XH_2^- (A) state is 0.31 eV more stable and 0.14 eV less stable than $H_2 + X^-$ for $X = B$ and Ga,

respectively.

Figure 1(c) shows a formation energy diagram where the chemical potential of all elements, μ_{ref} (see Sec. VIII: Methods) was chosen such that the origin of the energy scale corresponds to the $H_2 + X^- + h^+$ state. From this diagram we clearly recognize the negative- U ordering of donor and acceptor transitions of both BH_2 and GaH_2 complexes. Figure 1(c) also shows that in p-type material, XH_2^- (A) complexes are unstable and they are expected to either dissociate, or temporarily convert into XH_2^+ (D) upon hole capture (step 3a). The geometry ‘D’ of the donor state, $Si-H_{BC} X H_{BC}-Si$, notably differs from ‘A’ in that both H atoms sit approximately at bond-center sites next to X. The latter is under coordinated, *i.e.* connects to two Si atoms only. Preliminary results show that step 3a (hole capture by XH_2^- (A) accompanied by reconfiguration to XH_2^+ (D)) has a small barrier of the order of 0.1 eV.

From the above, the activation energy for $H_2 + X^- + 2h^+ \rightarrow XH_2^+$ along steps 1-2a-3a is estimated as 1.1 eV and 1.4 eV for $X = B$ and Ga, respectively. The B-related intermediate states along the reaction are also more stable than their Ga analogues. Hence, the formation of XH_2^+ complexes along this route is anticipated to be more favorable in B-doped than in Ga-doped Si.

Inspection of the one-electron structure of $XH-H^-$ reveals a deep fully occupied state within the gap, which could be responsible for trapping holes (step 2b), thus converting the H^- unit into H^0 or H^+ . The barrier for such capture processes is deemed small and it is neglected in the following analysis. From NEB calculations we obtained minute barriers ($\lesssim 0.2$ eV) for conversion of $XH-H^0$ into XH_2^0 (D). The latter state is 0.08 eV and ~ 0 eV above the $H_2 + X^- + h^+$ initial state for $X = B$ and Ga, respectively (see Figure 1(c)). Assuming that hole capture will readily bring the complex into the ground state XH_2^+ (D), we conclude that route along steps 1-2b-3b, is not only simpler, but its is also expected to involve lower barriers after the critical step 1. Our assessment is that route along steps 1-2b-3b is more likely to explain the conversion $H_2 + X^- + h^+ \rightarrow XH_2^+$, for which we have found effective activation barriers of 1.10 eV and 1.05 eV ascribed to step 1 for $X = B$ and Ga, respectively.

Although the dissociation of H_2 molecules assisted by B and Ga show almost identical activation energies (perhaps it is slightly more favorable when Ga is involved), the resulting BH_2^+ and GaH_2^+ show very different electrical activity. This finding was firstly reported in Ref. [29] and it is clearly shown by the formation energy diagram of Figure 1(c). Whereas BH_2^+ is a deep donor, GaH_2^+ is very shallow. Indeed, the wavefunction of the donor state of GaH_2^+ is very diffuse and spans the whole supercell. This is a strong indication that it is an effective-mass-like donor. Our conclusion is that while both BH_2^+ and GaH_2^+ are likely to form upon reaction of H_2 with B and Ga, the latter is unlikely to lead to strong carrier recombination activity.

We finally report on the dissociation mechanism of XH_2^+ complexes. This was partially addressed (for BH_2^+) in Ref. [24] and now we extend our analysis to GaH_2^+ . The jump of one of the H atoms in XH_2^+ into a neighboring Si-Si bond center site ($XH_2^+ \rightarrow XH-H^+$) involves surmounting a barrier

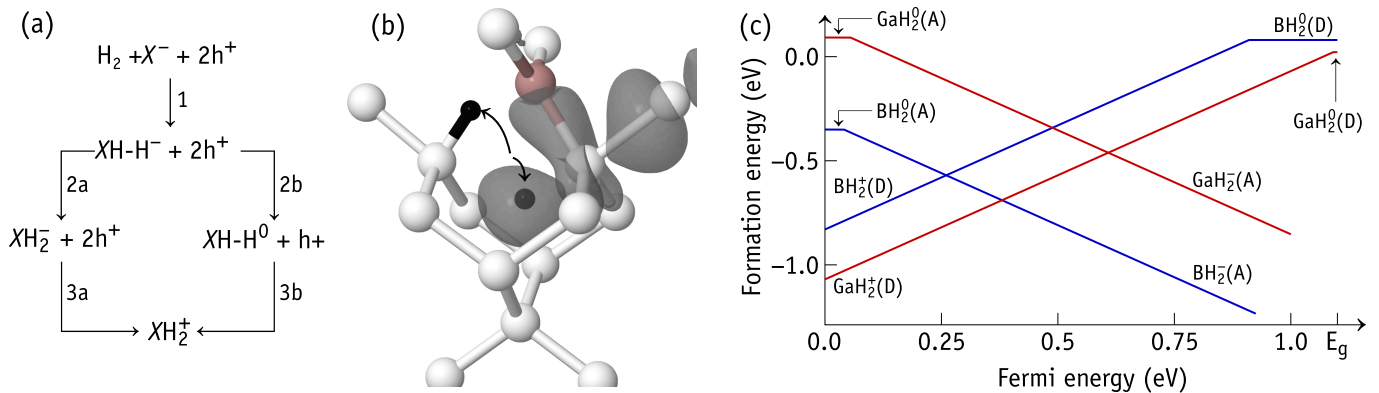


Figure 1. (a) Proposed mechanism for dissociation of H_2 molecules next to acceptor impurities in p-type silicon and subsequent formation of XH_2^+ complex. (b) Atomistic structure of the $GaH-H^-$ complex obtained after step 1, along with the electron density associated with the highest occupied gap state (gray isosurface), which is likely to trap holes. Si, Ga and H are shown in white, pink and black balls, respectively. The arrows depict an approximate trajectory of H atoms upon dissociation. (c) formation energy diagram of BH_2 and GaH_2 complexes in Si. The origin of the vertical axis corresponds to the state $H_2 + X^- + h^+$, where X is the corresponding acceptor.

of ~ 0.7 eV for both $X = B$ and Ga. These are lower than binding energies of $XH + H^+ \rightarrow XH_2^+$ (Table I) plus migration barrier of H^+ (calculated as 0.42 eV [25]). From here we arrive at 0.82 eV and 0.92 eV for dissociation energies via $XH_2^+ \rightarrow XH + H^+$ for $X = B$ and Ga, respectively. We conclude therefore, that both BH_2^+ and GaH_2^+ are intermediate byproducts along the reaction $H_2 + 2X^- + 2h^+ \rightarrow 2XH$. However, while BH_2 is suggested to be a non-radiative recombination center (linked to LeTID in B-doped cells), GaH_2 is likely to be harmless with respect to lifetime [29].

III. PHOSPHORUS-HYDROGEN PAIRS

We now look at reactions between hydrogen and phosphorus. In n-type silicon, atomic hydrogen is negatively charged and is readily attracted by P^+ ions to form PH pairs. Among more than 10 different locations for H next to P (up to third neighboring tetrahedral interstitial, bond-center and anti-bonding sites), we arrived at three prominently stable PH configurations. They are depicted in the upper part of Figure 2 and are referred to as PH_{AB} , PH_{BC1} and PH_{BC} . Other (less stable) configurations are schematically depicted in Figures S1 and S2 of Supporting Information. Their respective energies are also reported in Table S1 of the same document. In PH_{AB} ($\equiv P: Si-H$), H connects to Si along the anti-bonding direction leaving a three-fold coordinated phosphorous with a fully occupied lone-pair of electrons resonant with the valence band. In PH_{BC1} ($\equiv P-Si-H-Si$), H sits at the closest Si-Si bond-center site next to the P atom. The latter is four-fold coordinated. In PH_{BC} ($\equiv P: H-Si$) the H atom connects to Si, next to the electronic lone pair of P. Both PH_{AB} and PH_{BC} were extensively explored in the past, the former being generally accepted as the ground state [46, 48, 49, 53, 59, 60, 74].

Among the above geometries, only the ground state PH_{AB} displayed a clean band gap. Calculation of electronic transitions from total energies confirmed that PH_{AB} is electrically inert, chemically passivating the P dopant. The PH_{BC1}

defect has a high-lying and fully occupied level, responsible for $(0/+)$ and $(+/++)$ transitions at $E_c - 0.27$ eV and $E_c - 0.51$ eV, mostly localized on the $Si-H_{BC1}-Si$ unit. The PH_{BC} geometry also has a fully occupied level in the gap, but closer to the valence band top. The origin of the level stems from the overlap of the 1s electron of H with the P lone pair, raising the energy of the latter above the valence band top. From total energies we found a $(0/+)$ transition of PH_{BC} at $E_v + 0.29$ eV (no second donor transition was found).

Figure 2(a) shows a formation energy diagram for the PH pair in Si, where the relative energies of the three most stable configurations are graphically combined as a function of the Fermi energy (solid lines). The origin of the formation energy axis was chosen to be the $P^+ + H^-$ state (uncorrelated P^+ and H^- ions), so that binding energies are readily obtained. The diagram shows that PH pairs adopt a neutral PH_{AB}^0 ground state for a wide range of Fermi level positions, most notably for $E_F > 0.33$ eV. Importantly, the results cannot explain the observed interaction of PH pairs with minority carriers in n-type Si [55]. The works of Refs. [59, 60] suggested that the observed charge state changes of the pairs upon hole capture could be explained by conversion between stable PH_{AB}^0 and PH_{BC}^+ states. A requirement for this to be credible is that PH_{BC}^+ would have to be the ground state under illumination or current injection conditions, *i.e.*, there had to be a $(0/+)$ transition somewhere in the gap involving PH_{AB}^0 and PH_{BC}^+ . Nearly three decades ago there were no accurate methods to find that. However, current hybrid functionals, which avoid well known limitations of semi-local exchange-correlation treatments, allow us to evaluate transition levels with 0.1 eV-accuracy. Our findings, depicted in Figure 2(a), clearly do not support the proposed $PH_{AB}^0 \leftrightarrow PH_{BC}^+$ transformative model. The figure also shows that double positive charge states are not stable in n-type Si. That includes uncorrelated $P^+ + H^+$ pairs (dashed line), which are only expected to form in p-type material.

Another pillar of the transformative model is the assignment of the $PH_{BC}^0 \rightarrow PH_{AB}^0$ transformation barrier to the ob-

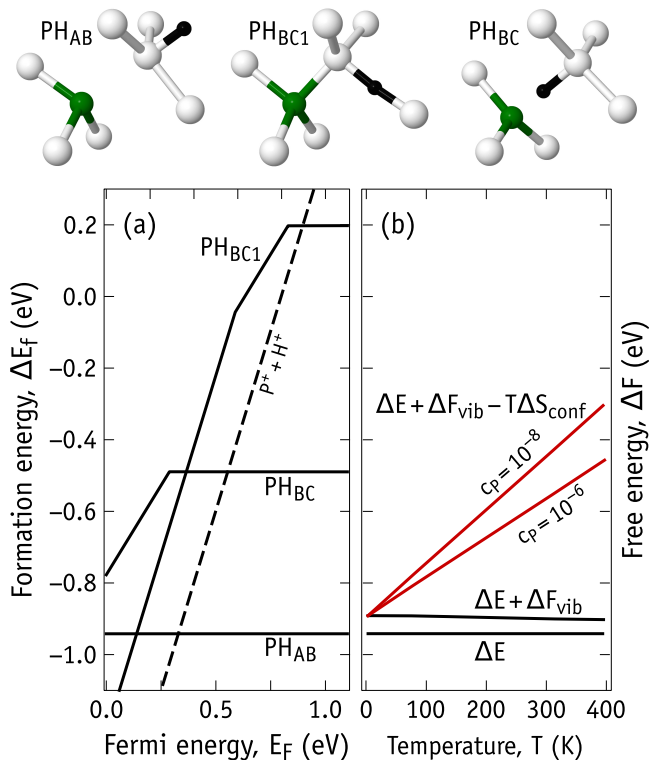


Figure 2. (Top) Atomistic structures of the most most stable PH complexes in Si in the neutral and positive charge states. Phosphorus, hydrogen and silicon are depicted in green, black and white, respectively. (a) Formation energy of PH complexes (solid lines) as a function of the Fermi energy. $E_F = 0$ at the valence band top. The dashed line represents the formation energy of infinitely separated P^{+} and H^{-} defects. (b) Helmholtz free energy change across the reaction $P^{+} + H^{-} \rightarrow PH$ in silicon (red lines). Potential energy (ΔE), vibrational Free energy (ΔF_{vib}) and configurational entropy ($-T\Delta S_{\text{conf}}$) contributions are represented in a cumulative way. Two doping concentrations are considered for the evaluation of S_{conf} , namely $c_P = 10^{-6}$ and 10^{-8} (see text). Both diagrams share the same vertical axis, with the origin representing the energy of infinitely separated H^{-} and P^{+} impurities.

served 0.7 eV activation energy of the passivation recovery kinetics of samples in darkness (which were previously illuminated) [58]. The interpretation was that under open-circuit and dark conditions, PH_{BC}^{+} complexes capture electrons, allowing them to return to their PH_{AB}^0 ground states. Our NEB calculations for this process give a barrier of 1.24 eV, a figure which is way too large to explain the recovery of resistivity at room temperature.

Another puzzle relates to the calculated binding energy $E_b = 0.94$ eV for $P^{+} + H^{-} \rightarrow PH$, which is larger than that of BH ($E_b = 0.76$ eV), in apparent contradiction with the higher thermal stability of the latter — whereas PH anneals out at about ~ 100 °C (in the dark) [47], the BH pairs dissociate in the range 140-200 °C [73].

Figure 2(b) represents the calculated Helmholtz free energy change $\Delta F = \Delta E + \Delta F_{\text{vib}} - T\Delta S_{\text{conf}}$ across $P^{+} + H^{-} \rightarrow PH$ as a function of temperature. Recent studies indicate that in

n-type Si (doping level 10^{15} cm^{-3}), H^{+} becomes the dominant species in thermal equilibrium at $T \gtrsim 400$ K [42, 43]. This is also an approximate upper limit for the thermal stability of PH. The graph is therefore limited to that temperature. For the evaluation of the free energy we considered changes in the all-electron potential energy (ΔE), vibrational free energy (ΔF_{vib}) and configurational entropy (ΔS_{conf}). The latter dominates the temperature dependence, accounting for $-T\Delta S_{\text{conf}} \approx 0.3$ -0.4 eV at room temperature. The configurational entropy change (per H atom) is approximated to $\Delta S_{\text{conf}} = k_B \ln(2c_P)$ [24], where k_B is the Boltzmann constant, and $c_P = n_P/n_{\text{Si}}$ is the fractional concentration of phosphorus donors, n_P and n_{Si} being absolute concentrations of P and Si atoms in the crystal. Figure 2(b) considers doping concentrations of $c_P = 10^{-8}$ ($n_P = 5 \times 10^{14}$ cm^{-3}) and $c_P = 10^{-6}$ ($n_P = 5 \times 10^{16}$ cm^{-3}). We note that for the evaluation of ΔS_{conf} we assume that the pairs are either all dissociated in the reactants side (high temperatures) or they are connected as PH_{AB} in the products side (low temperatures). It is also assumed that $n_H \ll n_P$ and there are no defect-defect interactions except for PH pair formation. The results are therefore qualitative. Although anharmonic effects are only expected to become relevant at $T \gtrsim 500$ K [75], we will argue that the lack of electron-phonon coupling is another limitation in the calculations.

According to Figure 2(b), at the observed annealing temperature of PH ($T \sim 350$ -400 K), the calculations indicate that the pair is still ~ 0.4 eV more stable than the $P^{+} + H^{-}$ state. This is owed to the large binding energy of the PH pair. The result contrasts with analogous calculations for BH, where the annealing temperature was estimated at $T \approx 450$ K [24], in fair agreement with experiments.

To address the above issues we investigated the potential energy surface of the H atom in the neighborhood of P. From the perspective of a charge state transition, the PH_{BC}^{+} geometry is rather distant from PH_{AB}^0 . Hence, we were particularly thorough in searching for a hole trapping mechanism involving structures closer to the PH_{AB}^0 ground state. We found that small wagging oscillations of the Si- H_{AB} unit of PH_{AB}^0 led to the appearance of an occupied gap level above the valence band edge. The oscillations are depicted schematically in Figure S1 of Supporting Information (for the H atom sitting on site 1). That particular movement and respective changes to the electronic structure were investigated using the NEB method.

Figure 3(a) shows potential energy diagrams for PH^0 and PH^{+} with their Si-H units performing a wagging movement. Figure 3(b) represents the corresponding position of the lowest unoccupied Kohn-Sham (LUKS) state of PH^{+} within the band gap as a function of the defect coordinate. Horizontal dashed lines at 5.31 eV and 6.83 eV of Figure 3(b) mark the energy of the highest occupied Kohn-Sham (HOKS) and LUKS states of a 216-atom bulk supercell at the Monkhorst-Pack special \mathbf{k} -point (folded $2 \times 2 \times 2$ grid). Note that these are not the band edges that define the indirect band gap as obtained from a primitive cell. Both diagrams of Figures 3(a) and 3(b) share the same horizontal axis, which represents the

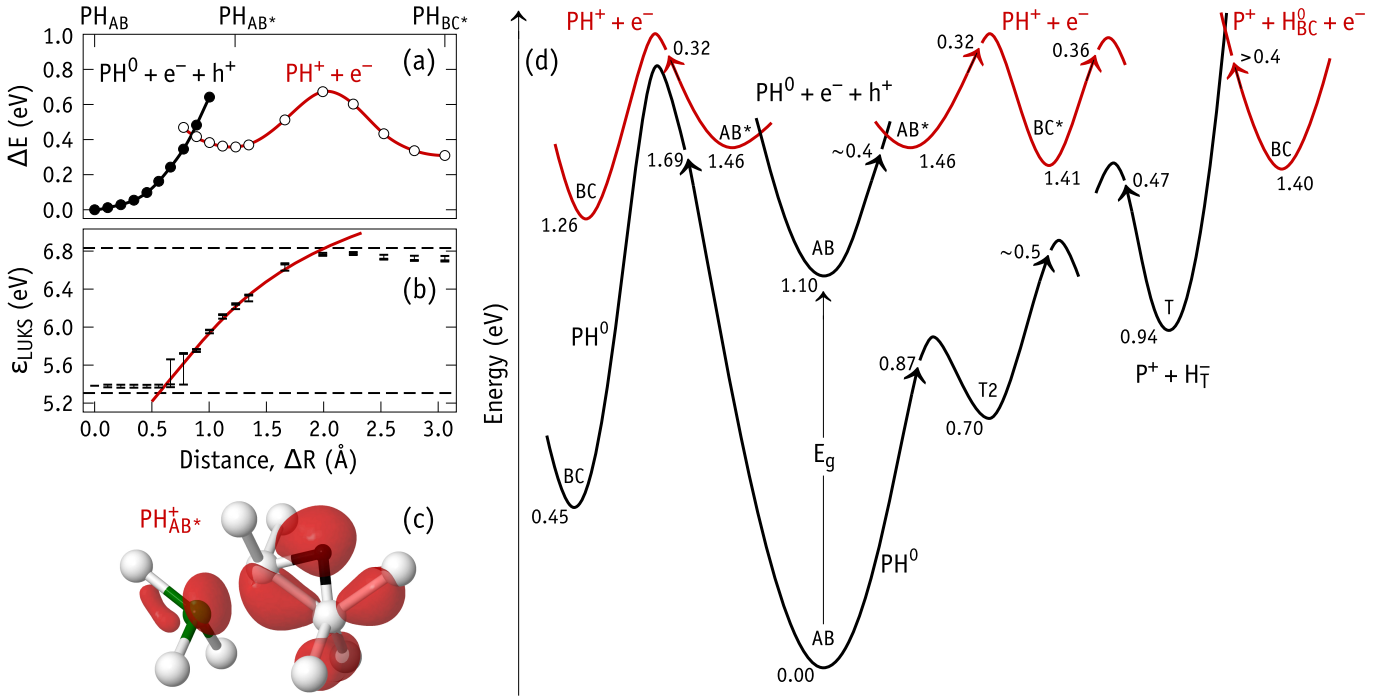


Figure 3. Proposed carrier-induced dissociation mechanism of PH pairs in silicon. (a) NEB calculation of the hole capture barrier for $\text{PH}_{\text{AB}}^0 + h^+ \rightarrow \text{PH}_{\text{BC}}^+$. Total energies of neutral and positively charged PH pairs are shown as filled and open circles. (b) Energy of the lowest unoccupied Kohn-Sham (LUKS) state of PH^+ . Defect geometries in (a) and (b) vary from those of PH_{AB}^0 ($\Delta R = 0$ Å) to PH_{BC}^+ ($\Delta R = 3.1$ Å) via PH_{AB}^+ (see text). The red line emphasizes the emergence of a hole trap about $\Delta R \sim 0.7$ Å, and it is drawn for the sake of eye guidance only. Dashed lines mark the HOKS and LUKS states in a bulk supercell. (c) Isosurface (red) of the hole localization in metastable PH_{AB}^+ state ($\Delta R \sim 1.2$ Å) calculated from the density of the LUKS state. P, H and Si atoms are depicted in green, black and white, respectively. (d) Configuration coordinate diagram describing interactions of PH pairs with carriers in n-type Si. Potential energy of neutral and positively charged pairs are shown as black and red lines, respectively. Defect geometries and respective energies are indicated next to the minima. Their lateral location in the diagram is not tied to a coordinate axis. The energy minima are calculated with respect to the PH_{AB}^0 ground state. The $\text{PH}_{\text{AB}}^0 + e^- + h^+$ state at $E_g = 1.10$ eV, represents a neutral PH defect plus an uncorrelated electron-hole pair. Energy barriers are represented next to the arrow heads (which indicate the direction of the reaction) and they are calculated with respect to the closest minima.

cumulative distance traveled by all atoms (mostly by H). In the present context, the LUKS of PH^+ stands for the state where a hole has been trapped. In Figure 3(b) we can notice up to three closely spaced horizontal bars for each geometry. They refer to the LUKS states for all symmetry-irreducible \mathbf{k} -points among the $2 \times 2 \times 2$ grid (see Methods section). Their spacing gives us an idea of the dispersion of the level in the BZ.

The itinerary of the wagging motion is $\text{AB} \rightarrow \text{AB}^* \rightarrow \text{BC}^*$ (and back). The AB^* and BC^* geometries ($\equiv \text{P: Si-H}_{\text{AB}}^*$ and $\equiv \text{P-Si-H}_{\text{BC}}^* \text{-Si} \equiv$), are metastable positive charge states, consisting of increasingly bent Si-H and Si-H-Si units next to a three-fold and four-fold coordinated P atoms, respectively. The PH_{BC}^+ state is already close, but still separated from PH_{BC1}^+ by a small barrier (0.36 eV high). The less distorted PH_{AB}^+ metastable structure is very close to that of PH_{AB}^0 , and the localization of the trapped hole is represented in Figure 3(c).

Figure 3(a) depicts the only route that we found for the trapping of holes by PH_{AB}^0 . It involves overcoming a capture barrier of ~ 0.4 eV before attaining PH_{AB}^+ ($R \approx 1.2$ Å). Figure 3(b) shows that the hole trap mixes with the valence band

top, and emerges at $R \gtrsim 0.7$ Å. Hence, a large cross-section for holes is expected (not for electrons). After arriving at PH_{AB}^+ (Figure 3(c)), several competing processes can follow, including hole re-emission, $\text{PH}_{\text{AB}}^+ \rightarrow \text{PH}_{\text{AB}}^0 + h^+$, or H jumps into PH_{BC}^+ , PH_{BC1}^+ or even PH_{BC}^+ . In the first case, the estimated emission barrier is ~ 0.1 eV and the defect returns to the neutral ground state. Regarding the H jumps, the barriers were calculated in the range 0.32-0.36 eV. These are rather low barriers, which should be easily surmounted at room temperature, and ultimately lead to $\text{PH}^+ \rightarrow \text{P}^+ + \text{H}^0$ dissociation.

So far, none of the PH^+ states presented (with BC^* , BC1 or BC geometries), are more stable than $\text{PH}_{\text{AB}}^0 + h^+$, so we still do not have an explanation for the photo- or current-induced dissociation of the PH pairs. For that, there must be a state, which is more stable than PH_{AB}^0 under illumination, and less stable in the dark. We propose that finite temperature effects could explain the existence of such state. From the all-electron energy calculations, we find that the photo-/injection-induced dissociation $\text{PH}_{\text{AB}}^0 + h^+ \rightarrow \text{P}^+ + \text{H}_{\text{BC}}^0$ has a potential energy cost of $\Delta E_R = 0.30$ eV. If we account for the configurational entropy raise of that reaction, we find that already near room temperature, $-T\Delta S_{\text{conf}} \approx -(0.3-0.4)$ eV,

meaning that the free energy of dispersed $P^+ + H^0$ becomes lower than that of the pairs, hence providing favorable conditions for the dissociation. On top of that, under persistent illumination, a second hole capture via $PH_{BC1}^+ + h^+ \rightarrow PH_{BC1}^{++}$ or via $P^+ + H^0 + h^+ \rightarrow P^+ + H^+$ (dashed line in Figure 2(a)), would lead to a further drop in the energy and to Coulomb repulsion between P^+ and H^+ , further enhancing of the dissociation rate.

Figure 3(d) shows a configuration coordinate diagram that summarizes our results for the PH pair in n-type Si. These diagrams are usually accompanied by a horizontal axis referring to a generalized coordinate. It would be meaningless, if not erroneous, to locate so many different geometries against a single axis. Hence, for the sake of diagram sanity, the coordinate axis is not shown, although the identification of each geometry is included next to each potential energy minimum.

Ground state potentials of close pairs (PH^0) and uncorrelated P^+ and H^- ions ($P^+ + H_T^-$) are shown at the bottom and right-hand side of the diagram, respectively. At the top we find an excited state corresponding to the generation of a free electron-hole pair ($PH^0 + e^- + h^+$) and states that result from thermally assisted capture of a minority carrier ($PH^+ + e^-$). Relative energies with respect to ground state PH_{AB}^0 are indicated next to the potential minima. Also indicated are several potential energy barriers for processes of interest (next to the arrow heads). These energies are relative to the nearest minimum. Finite temperature effects (not represented), most notably from configurational entropy, stabilize the states on the right hand side of the diagram, namely $P^+ + H_{BC}^0 + e^-$ and $P^+ + H_T^-$.

At room temperature and darkness, the ground state is the PH_{AB}^0 passivated pair. Conversion to metastable PH_{BC}^0 involves surmounting a ~ 1.7 eV barrier, which is even higher than the dissociation barrier (1.41 eV). However, when minority carriers (holes) are present and some heat is provided, a thermally-assisted capture $PH_{AB}^0 + h^+ \rightarrow PH_{AB^*}^+$ may occur with a capture barrier of about 0.4 eV. This provides the opportunity of H^0 to quickly jump away from P^+ , and find a more stable state with larger entropy.

The diagram also shows that from $PH_{AB^*}^+$, the defect can be converted to PH_{BC}^+ by overcoming a barrier of only 0.32 eV (toward the left hand side of the excited state potential). From here, it could capture an electron and become trapped at the relatively deep potential of PH_{BC}^0 . However, this picture cannot explain the increase of fixed charges observed during light-soaked annealing treatments of hydrogenated diodes (re-activation of $P^+ + e^-$).

Our calculations support a dissociative model for the observed light-/current-induced changes of PH pairs in Si. After dissociation of PH, and if darkness is restored, any metastable H_{BC}^0 will relax to H_T^- after electron capture. This step must be preceded by a reconfiguration of H from the bond center site into a tetrahedral cage of the crystal, surmounting a barrier of about 0.4 eV [25]. That is our estimated lower bound for the capture barrier of $H_{BC}^0 + e^- \rightarrow H_T^-$ (right hand side of the diagram). The recovery of the pairs then involves the migration of isolated H^- toward the P^+ ions (with a calculated 0.47 eV jumping barrier). This result is in line with the find-

ings of Johnson and Herring [58], which found an activation energy of 0.7 eV for the whole recovery process. We note that the measured barrier can be related (but not exclusively) to an activation energy for the release of H^- from a trapping site (e.g. interstitial oxygen), and as emphasized in Ref. [58], the measured figure represents an upper bound for the migration barrier of H^- .

The thermally-assisted capture mechanism $PH_{AB}^0 + h^+ \rightarrow PH_{AB^*}^+$ leads us to postulate that the thermal stability of the PH pairs, which is considerably lower than that of BH pairs, could be limited by interactions with intrinsic carriers. At 100 °C the intrinsic hole concentration is already $1.5 \times 10^{12} \text{ cm}^{-3}$ [76], and their capture could accelerate PH dissociation by (1) providing a low-barrier escape route for H (the neutral state is expected to travel much faster than H^-), (2) turning off the Coulomb attraction between hydrogen and phosphorus, and (3) attaining a higher entropy state in the presence of a steady-state hole population. This mechanism differs markedly from the dissociation of the BH pair. In that case, close B^- and H^+ units are electrically inactive, even when separated by a few Si-Si bonds [24], implying that any light/injection-induced enhancement of BH dissociation occurs only after enough separation of the pairs is verified, which requires considerable heat to be provided ($T \gtrsim 180$ °C) [77].

We finally note that a more rigorous account of the above picture would include the calculation of the capture cross section for $PH_{AB}^0 + h^+ \rightarrow PH_{AB^*}^+$. That involves finding the hole capture rate and the respective electron-phonon matrix elements [78–80]. This is outside the scope of the present work. Importantly, our results suggest that the PH pair, although it is electrically inert from the perspective of a static calculation, that may not be the case if we account for electron-phonon coupling.

IV. INTERACTIONS OF HYDROGEN MOLECULES WITH PHOSPHORUS

From several geometries (up to 10 pair combinations of H sites as depicted in Figs. S1 and S2 of Supporting Information) and charge states ($q = \{-1, 0, +1\}$) of complexes that result from reaction $P^+ + H_2 + (1-q)e^- \rightarrow PH_2^q$ between P and H_2 , we could only find two stable configurations with $\Delta E_R \lesssim +1$ eV. Their geometry consists of H pairs at sites 3-5 and 1-3 shown in Fig. S1 of Supporting Information. They are analogous to XH_2^- (A) complexes (X is a group-III acceptor), but now a Si-P bond is either replaced by Si- H_{BC} P- H_{AB} or by H_{AB} -Si H_{BC} -P. Both structures display trigonal (C_{3v}) point group symmetry, they show close stability (the former is more stable by 0.2 eV only), and because P is four-fold coordinated (Si and H have their *normal* coordination), both PH_2 defects are shallow donors. We can therefore already presume, that unlike BH_2 complexes which were suggested to be responsible for LeTID in B-doped Si, formation of PH_2 complexes is unlikely to result in strong recombination activity.

Although we did not investigate the dissociation mechanism of H_2 molecules next to P^+ dopants (as we did for B^- and Ga^- acceptors), we could find that such reactions are not

Table II. Calculated reaction energies (ΔE_R) for formation of phosphorus-hydrogen complexes in n-type silicon. All values are in eV.

Reaction	ΔE_R
$P^+ + H_2 \rightarrow PH_2^+$	+0.06
$PH_{AB}^0 + H_T^- \rightarrow PH_2^+ + 2e^-$	-0.40
$2PH_{AB}^0 \rightarrow PH_2^+ + P^+ + 2e^-$	+0.47
$2P^+ + H_2 + 2e^- \rightarrow P^+ + PH_{AB}^0 + H_T^-$	+0.46
$2P^+ + H_2 + 2e^- \rightarrow 2PH_{AB}^0$	-0.41

very favorable and some are actually endothermic. PH_2 complexes are expected to be thermally ionized at room temperature and above, and hence, for the sake of reaction analysis, they are considered in the positive charge state. The results are summarized in Table II. The first three rows account for reactions involving the formation of PH_2^+ (in the most stable Si- H_{BC} P- H_{AB} form). The reaction between H_2 and P^+ in the first row is endothermic, $\Delta E_R = +0.06$ eV, and that still excludes the fact that $\Delta S_R < 0$, which makes the reactants even more stable at finite temperatures. The reaction in the second row shows that free H^- can be trapped by PH pairs (with a binding energy of 0.40 eV). However, this can only occur transiently, and when the concentration of PH pairs is much higher than that of P^+ ions. Otherwise, as shown by the result of the third row, each PH_2 complex will eventually dissociate to form PH pairs (with 0.47 eV gain per PH_2 complex).

Another important question is: what does theory anticipate for the energetics of PH pair formation from interactions between H_2 and P^+ ? The answer is partially found in the last two rows of Table II. The first indicates that there is a barrier for the full conversion, which is greater than ~ 1 eV (*i.e.* 0.46 eV plus the migration barrier of H^-). The last row shows that a full reaction between H_2 and P^+ donors,



is exothermic, although it does not lead to a substantial potential energy drop ($\Delta E_R = -0.41$ eV). Of course, at finite temperatures, and most importantly in the solar context, at room temperature and above, several factors are expected to play against the above reaction. These include changes in configurational entropy, electronic free energy (due to subtraction of two free-electrons), rotational and vibrational free energies (consumption of the H_2 molecules), as well as the capture of photogenerated holes by PH.

Let us first estimate the configurational entropy change. For Reaction 2 this quantity can be approximated to $\Delta S_{\text{conf}} = k_B [\ln(8c_P^2/c_H) + 1]$ (see Appendix B of Ref. [24]), and for instance, choosing fractional concentrations $c_P = 10^{-7}$ and $c_H = 10^{-10}$ ($n_P = 5 \times 10^{15} \text{ cm}^{-3}$ and $n_H = 5 \times 10^{12} \text{ cm}^{-3}$), we find $(-300 \text{ K}) \times \Delta S_{\text{conf}} = 0.16$ eV and $(-400 \text{ K}) \times \Delta S_{\text{conf}} = 0.21$ eV.

The raise in the Helmholtz electronic free energy across the reaction is estimated from $\Delta F_{\text{elec}} \approx f(\mu - k_B T)$, which subtracts $pV = k_B T$ (for an ideal electron gas) to the Gibbs free

energy per free-electron $\mu \approx k_B T \ln(\Delta n/N_C)$ (see Ref. [75]), where $\Delta n = fn_H$ is the effective change in the free-electron density, $f = \exp(-E_i/k_B T)$ is a Boltzmann factor quantifying the effective fraction of thermally ionized phosphorus donors with ionization energy E_i , and N_C is the effective density of states at the bottom of the conduction band. From the above, we find $\Delta F_{\text{elec}} = 0.12$ eV and 0.24 eV at $T = 300$ K and 400 K, respectively, meaning that even without considering the roto-vibrational contribution of the molecule, the free energy change $\Delta F = \Delta E_R + \Delta F_{\text{elec}} - T\Delta S_{\text{conf}}$ across Reaction 2 is nearly zero at room temperature.

Our results suggest that after cooling P-doped Si that was in contact with a high-temperature hydrogen source, *e.g.* after a fast-firing step for contact formation during solar cell fabrication, PH pair formation is unlikely to occur at the expense of direct reactions between H_2 molecules and P^+ . This conclusion is indirectly supported by the measurements of Pritchard *et al.* [18], who followed the detachment of H_2 molecules from interstitial oxygen defects (which act as trapping sites) in P-doped Czochralski Si samples, showing a concomitant increase of free H_2 located at tetrahedral interstitial sites of the crystal. The conversion was monitored during annealing treatments between room temperature and $T = 130$ °C, there was no indication of PH pair formation in the initial state (*as-quenched*) of the samples, and the conversion from trapped to free H_2 was complete, irrespectively of the temperature. This contrasts with analogous experiments in B-doped material, where a substantial fraction of H was already present in the form of BH pairs after quenching the samples (previously put in contact with an H_2 gas at 1200 °C) to room temperature [19].

V. HYDROGEN REACTIONS WITH CARBON

Here we have a look into several open issues related to carbon-hydrogen complexes in Si, especially regarding their formation, dissociation, and their electronic activity. Interactions between hydrogen and substitutional carbon is likely to occur in solar-grade Si, where the concentration of substitutional carbon can reach 10^{16} cm^{-3} . Complexes that result from hydrogenation of substitutional carbon pairs (C_2H_n) are only expected in C-rich material, and they are left outside the scope of the present work.

We first focus on the CH pair. According to our results the $\equiv C-H_{BC}$ Si \equiv configuration (referred to as CH_{BC} and shown in Figure 4(a)), is the most stable for charge states +, 0 and -. These possess a Si dangling bond with electron occupancy of 0, 1 and 2 electrons, respectively. The alternative structure $H_{AB}-C$ Si \equiv (referred to as CH_{AB} , and also showing four- and three-fold coordinated C and Si atoms, respectively) is 0.71, 0.41 and 0.17 eV above CH_{BC}^+ , CH_{BC}^0 and CH_{BC}^- ground states, respectively. These results are in line, but also improve upon previous local density approximated calculations [69, 81]. Like in Ref. [69], we also found low energy configurations for CH^+ and CH^- where H is not directly attached to the C atom. The positive metastable state consists of a Si- H_{BC}^+ -Si unit next to substitutional carbon (0.21 eV above the

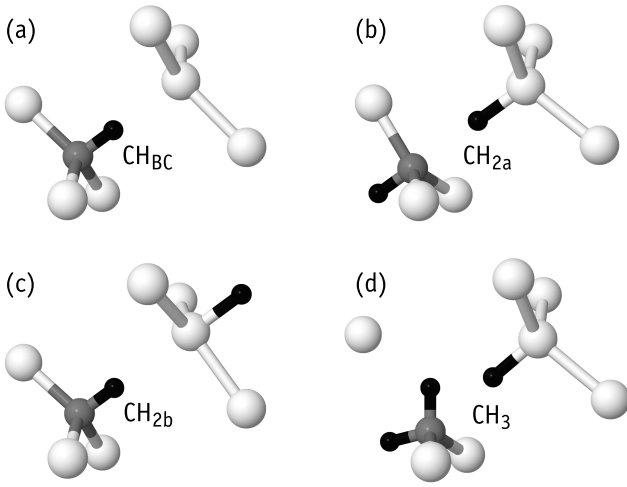


Figure 4. Atomistic structures of the most most stable CH_n complexes in Si ($n \leq 3$). Carbon, hydrogen and silicon are depicted in gray, black and white, respectively. $\Delta E_R = E_{fs} - E_{is}$ and $\Delta E_A = E_{ts} - E_{is}$, where subscripts ‘is’, ‘ts’ and ‘fs’ stand for initial, transition and final states of the reaction on the leftmost column, respectively. All values are in eV.

CH^+ ground state). This is hereafter referred to as CH_{BC1}^+ . The negative metastable state is attained when H sits close to the tetrahedral interstitial site next to C along the $\langle 100 \rangle$ direction (0.20 eV above the CH^- ground state). This state is analogous to that of site 10 in Figure S1 of Supporting Information, and it is referred to as CH_{T1}^- .

The binding of free hydrogen ions to carbon in p-type and n-type Si ($\text{H}^+ + \text{C} \rightarrow \text{CH}^+$ and $\text{H}^- + \text{C} \rightarrow \text{CH}^-$) is favored by $\Delta E_R = -0.41$ eV and -0.71 eV, respectively. These values contrast with the not so favorable reaction energies to produce CH upon interaction of H_2 molecules with C (first three rows of Table III). Such difference could explain why CH complexes form underneath the surface of wet-etched or H-plasma treated Si, but as far as we are aware, no one has reported their appearance after cooling hydrogenated Si from above ~ 700 °C (a procedure which promotes the formation of H_2 molecules).

Interestingly, we found that $\text{BH} + \text{C} \rightarrow \text{B}^- + \text{CH}_{\text{BC}}^+$ and $\text{PH} + \text{C} \rightarrow \text{P}^+ + \text{CH}_{\text{BC}}^-$ are endothermic with $\Delta E_R = +0.46$ and $+0.70$ eV, respectively (see Table III). These figures tell us that CH pairs cannot be formed at the expense of dopant-hydrogen pairs.

The calculated donor and acceptor transitions for CH_{BC} are estimated at $E_v + 0.37$ eV and $E_c - 0.10$ eV, respectively. The acceptor level agrees well with the E3 electron trap at $E_c - 0.16$ eV, measured by DLTS in n-type Si by Kamiura *et al.* [70] (also referred to as (C-H)_{II} in Ref. [69] and E90 in Ref. [72]), whereas the calculated donor transition fits well the H1 hole trap also measured by DLTS at $E_v + 0.33$ eV, and assigned to a CH defect [71] (also labeled H180 in Ref. [72]). Although the H1/H180 hole trap did not show a shift of the emission rate with varying the bias (as it is expected for a donor in p-type Si) [71], the existence of a capture barrier of

~ 0.05 eV led to the suggestion that it should be an acceptor [72]. Our results do not support this view.

DLTS and C-V measurements of wet-etched B-doped samples show that H180 and BH pairs have the same depth profile [82], thus suggesting that both also have the same number of hydrogen atoms. The H1 trap was shown to anneal out in the dark above 100 °C with an activation energy of 1.7 eV. From NEB calculations, we find that a $\text{CH}_{\text{BC}}^+ \rightarrow \text{CH}_{\text{BC1}}^+$ jump has a barrier of 1.61 eV. Assuming that subsequent H^+ jumps into farther Si-Si bonds have lower barriers, we find in this result further support for the assignment of H1 to the donor transition of CH_{BC} .

Additional NEB calculations were performed to understand the dissociation of CH_{BC} . In the neutral charge state, the H jump with the lowest barrier (that is not a reorientation) was also $\text{CH}_{\text{BC}}^0 \rightarrow \text{CH}_{\text{BC1}}^0$, with the saddle point at 1.41 eV above the initial state. On the other hand, in the negative charge state the easiest first step for dissociation was found $\text{CH}_{\text{BC}}^- \rightarrow \text{CH}_{\text{T1}}^-$, with a much lower potential energy barrier, estimated as 0.66 eV. These figures match very well the activation energies for annealing of the E3 electron trap in n-type Si diodes under (1) bias and darkness and (2) at zero-bias under white light illumination [70]. In (1) the Fermi level was well below the $E_c - 0.16$ eV acceptor level and the defect did not have access to free electrons. Under these conditions, E3 defect traps were empty (here interpreted as the CH_{BC}^0 state) and it was shown to take days to anneal them out at ~ 60 °C. An activation energy of 1.33 eV (with a pre-factor of 10^{14} s^{-1}) was extracted from isothermal annealing data assuming first-order and Arrhenius behavior. That is very close to the calculated barrier for $\text{CH}_{\text{BC}}^0 \rightarrow \text{CH}_{\text{BC1}}^0$ and the pre-factor suggests that the mechanism involves simple atomic motion. In (2), the E3 traps had access to a non-equilibrium population of photogenerated electrons and they annealed out in a time-scale of minutes, even below room temperature. The annealing rate under these conditions was estimated as $10^6 \text{ s}^{-1} \times \exp(-0.5 \text{ eV}/k_B T)$. Now the barrier is close to that of $\text{CH}_{\text{BC}}^- \rightarrow \text{CH}_{\text{T1}}^-$, and the pre-factor suggests that an electron is captured by CH_{BC}^0 before performing the jump.

The CH_{BC1} defect has also been investigated before in n-type Si [69]. For this defect we find a calculated donor transition at $E_c - 0.22$ eV. Hence, we support its assignment to an electron trap labeled (C-H)_I (a precursor to (C-H)_{II}), measured at $E_c - 0.22$ eV, showing a clear Poole-Frenkel behavior, and ascribed to a Si-H-Si defect next to a carbon atom [69].

As mentioned already, CH_{AB} and CH_{T1} geometries are quite stable in the negative charge state (0.17 eV and 0.20 eV above CH_{BC}^-). Like CH_{BC1}^+ in proton-implanted Si, they could be precursors to the CH_{BC}^- ground state, especially in n-type wet-etched Si. For CH_{AB} we find (0/+) and (-/0) transitions at $E_v + 0.08$ eV and $E_c - 0.31$ eV. These are about 0.2 eV lower in the gap than the analogous levels of CH_{BC} . This shift toward lower energies can be explained by the absence of repulsion between the 1s state of H (which is now at the anti-bonding site) and electrons on the Si radical state. The calculated levels are also in line with transitions arising from other Si dangling bond defects, *e.g.*, VOH with donor and acceptor transitions at $E_v + 0.28$ eV and $E_c - 0.31$ eV [83]. The low-

Table III. Calculated reaction energies (ΔE_R) involving several carbon-, boron, and phosphorus-hydrogen complexes in silicon. All values are in eV.

Reaction	ΔE_R
$\frac{1}{2}\text{H}_2 + \text{C} \rightarrow \text{CH}$	+0.12
$\frac{1}{2}\text{H}_2 + \text{C} + \text{h}^+ \rightarrow \text{CH}^+$	-0.25
$\frac{1}{2}\text{H}_2 + \text{C} + \text{e}^- \rightarrow \text{CH}^-$	+0.02
$\text{H}_2 + \text{C} \rightarrow \text{CH}_2$	-0.97
$\frac{3}{2}\text{H}_2 + \text{C} \rightarrow \text{CH}_3$	-0.90
$\text{BH} + \text{C} \rightarrow \text{B}^- + \text{CH}^+$	+0.46
$\text{PH} + \text{C} \rightarrow \text{P}^+ + \text{CH}^-$	+0.70
$2\text{BH} + \text{C} \rightarrow 2\text{B}^- + \text{CH}_2 + 2\text{h}^+$	+0.35
$2\text{PH} + \text{C} \rightarrow 2\text{P}^+ + \text{CH}_2 + 2\text{e}^-$	+0.49
$\text{BH} + \text{CH}_2 \rightarrow \text{B}^- + \text{CH}_3^+$	+0.35
$\text{PH} + \text{CH}_2 \rightarrow \text{P}^+ + \text{CH}_3^0 + \text{e}^-$	+0.80

est unoccupied electronic state of CH_{AB}^- is a conduction band state, and as expected, no second acceptor level was found for this geometry.

As for CH_{T1} we find a $(-/0)$ level at $E_v + 0.19$ eV. Also for this defect, the calculations suggest that it cannot trap a second electron (it is a single acceptor). Judging from the estimated error bar of these calculations (~ 0.1 eV), we are not able to connect any of the calculated levels of CH_{AB} and CH_{T1} defects to other observed traps that were convincingly shown to be C-H related [72]. Perhaps the $(-/0)$ level estimated at $E_c - 0.31$ eV for CH_{AB} is not that far from the observed deep electron trap at $E_c - 0.51$ eV (labeled E262) [84]. Such discrepancy could in principle be explained by the existence of an unusually large capture barrier ($\gtrsim 0.1$ eV) for $\text{CH}_{\text{AB}}^0 + \text{e}^- \rightarrow \text{CH}_{\text{AB}}^-$ which was not considered theoretically. However, E262 was shown to be accompanied by another trap (labeled E46) at 0.06 eV below E_c , both displaying identical depth profiles to that of the PH pair, showing similar annealing behavior, and also showing identical dependence on the carbon concentration [84]. For that, E262 and E46 were assigned to first and second acceptor transitions of the same complex, possibly CH_{AB} . Our calculations seem to rule out that possibility.

VI. HYDROGEN MULTI-TRAPPING AT CARBON

Substitutional carbon in Si is known to trap at least two hydrogen atoms. This effect has been found both in proton implanted material [85], and in Si samples heated above 1300 °C in a H_2 -rich atmosphere and quenched to room temperature [65]. As for modeling the CH_2 complexes, that was extensively addressed by Estreicher and co-workers [68, 86]. Like for the PH_2 complexes, there are two stable configurations for CH_2 . They are shown in Figures 4(b) and 4(c), and we confirm that they are nearly degenerate and electrically inert. Their detection relies on local vibrational mode spectroscopy only [65, 85].

Table III shows few possible reactions leading to formation of CH_2 , where we can find a substantial potential energy drop for $\text{H}_2 + \text{C} \rightarrow \text{CH}_2$ ($\Delta E_R = -0.97$ eV). This reaction was studied in detail in Ref. [24], where it was found that like boron, carbon can enhance the dissociation of H_2 molecules (dissociation barrier of 1.35 eV). However, unlike B, the state attained after dissociation, Si-H H-Si, is electrically inert and subsequent steps cannot benefit from the capture of carriers.

Like for the CH pair, formation of CH_2 upon release of H from PH in n-type and BH in p-type Si is not favorable, *i.e.*



and



are endothermic reactions. This suggests that CH_2 cannot be obtained upon annealing of BH and PH pairs. Similar conclusions can be drawn for the formation of CH_3 complexes (see Table III). The latter complex is not even stable against decomposition into CH_2 plus a dopant-hydrogen pair. The most stable form of CH_3 is depicted in Figure 4(d), and comprises a Si radical next to $=\text{CH}_2$ and $\equiv\text{SiH}$ units. A deep donor transition was calculated at $E_v + 0.43$ eV (no acceptor levels were found), and also in this case, we cannot find a match with any of the DLTS traps summarized in Table 1 of Ref. [72], in particular with the one labeled E90' at $E_c - 0.14$ eV assigned to a CH_n defect with $n > 1$.

VII. CONCLUSIONS

We presented a comprehensive theoretical study of hydrogen-dopant and hydrogen-carbon interactions in silicon using state-of-the-art electronic structure methods. The impact and role of several hydrogen-related complexes was addressed in the context of non-radiative recombination of carriers by defects in solar silicon, in particular of LeTID of Si cells.

The interaction of H_2 molecules with B and Ga acceptors was investigated comparatively. We found that both $X = \{\text{B}, \text{Ga}\}$ group-III elements act as catalysts for H_2 dissociation, leading to formation of intermediate XH_2^+ complexes before attaining a lower energy state consisting of acceptor-hydrogen pairs (XH). The activation energy of the acceptor-assisted dissociation of H_2 is estimated 1.10 eV and 1.05 eV for B and Ga (to be compared with 1.6 eV for H_2 dissociation in pristine Si). These values are close to the activation energy for the LeTID development in Si cells. These barriers are also the critical steps for formation of BH_2^+ and GaH_2^+ along $\text{H}_2 + 2\text{X}^- + 2\text{h}^+ \rightarrow \text{XH}_2^+ + \text{X}^- \rightarrow 2\text{XH}$. The BH_2^+ was previously assigned to the route-cause of LeTID in B-doped solar cells. However, GaH_2^+ are effective-mass-like shallow donors, and therefore, unlikely to lead to analogous recombination activity in cells based on Ga-doped substrates.

We find that light-carrier-induced dissociation of PH pairs cannot be explained by a transformative model, where H

jumps between anti-bonding and bond-center sites upon capture of minority and majority carriers. Instead, our results suggest a dissociative mechanism, triggered by a metastable hole trap accessible to the ground state via wagging vibrations of the Si-H_{AB} unit. From there, the height of the potential energy barriers for H detachment are a few tenths of eV only, and H can either escape as H⁰ or as H⁺ if it captures another hole. In the latter case, the escape would be enhanced by the repulsive field of P⁺. Interestingly, the above model suggests that a defect, which according to a static calculation does not have electrical levels in the gap, is still capable of trapping free carriers, but that can only be explained if we account for electron-phonon coupling and finite temperature effects.

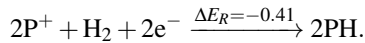
Indeed, an important contribution to the dissociation of PH is the raise of configurational entropy. At $T = 300$ K and in the presence of minority carriers, the magnitude of $-T\Delta S_{\text{conf}}$ makes the reaction,



more likely and a subsequent electron capture by hydrogen leads to further stabilization. The above mechanism for minority carrier enhanced dissociation of PH could explain why its annealing temperature is ~ 100 °C lower than that of BH pairs, despite the smaller binding energy of the latter. With respect to that, we suggest that PH dissociates above $T \approx 100$ °C in the dark with help of the increasing concentration of intrinsic holes.

Interactions between H₂ molecules and phosphorus was also investigated. Direct interactions via $\text{H}_2 + \text{P}^+ \rightarrow \text{PH}_2^+$ are not favorable ($\Delta E_{\text{R}} = +0.06$ eV). Although the products are the most stable form of PH₂, they are shallow donors, and even if they could form, they are not expected to lead to recombination activity, not even to changes in conductivity.

We found that PH pair formation at the expense of H₂ molecules and P donors leads to a small energy drop of $\Delta E_{\text{R}} = -0.4$ eV, i.e.,



However, we also find that configurational and electronic entropy alone (without considering roto-vibrational contributions from the H₂ molecule, which favors the reactants side), are able to cancel ΔE_{R} at $T \gtrsim 300$ -400 K. This result suggests that PH formation from direct interactions between H₂ and P⁺ is unlikely during the cooling of n-type solar cells subject to fast-firing treatments.

We also explored the details of mechanisms behind the annealing of CH pairs under dark conditions and under white light illumination (or carrier injection). Strong differences stem from different barriers and jump mechanisms as a function of the charge state. For CH⁺, CH⁰ and CH⁻, dissociation barriers were estimated as 1.61 eV, 1.41 eV and 0.66 eV, respectively. These quantities agree fairly well with the available experimental data, shedding light into an old and unsolved puzzle. We confirm the assignment of two measured carrier traps (H1[71] and E3/(C-H)_{II}/E90 [69, 70, 72]) to electronic transitions involving the most stable configuration of

the CH pair. The calculation of a metastable donor transition involving a C-Si-H-Si structure (reminiscent of the (0/+)) transition of isolated bond-centered hydrogen), also supports its previous assignment to the (C-H)_I electron trap [69].

CH_n complexes are not stable against formation of dopant-H pairs. They could however form transiently in C-rich Si, *e.g.*, under solar cell operating conditions due to light-enhanced dissociation of dopant-H complexes. The CH pair in p-type Si is positively charged, it is stable above room temperature, and could act as a non-radiative recombination center by attracting minority carriers (photo-generated electrons). It is therefore a suspect to consider as LeTID defect in cells based on B- and Ga-doped substrates. CH₂ is electrically inert and CH₃, although has a deep donor level, it is unstable and unlikely to form.

VIII. METHODS

We employed the density functional Vienna Ab-initio Simulation Package (VASP) [87–89], which uses the projector-augmented wave method [90] and planewaves for the description of core and valence electronic states, respectively. The maximum kinetic energy of the planewaves was 400 eV. Total energies were evaluated self-consistently, using the hybrid density functional of Heyd-Scuseria-Ernzerhof (HSE06) [91, 92], with a numerical accuracy of 10^{-6} eV. Mixing and screening parameters were those originally proposed for this functional ($a = 1/4$ and $\omega = 0.2 \text{ \AA}^{-1}$) [92], leading to an indirect band gap in the Kohn-Sham band structure of about 1.1 eV. All-electron energies were found for defective supercells of Si, constructed by replication of $3 \times 3 \times 3$ conventional unit cells with theoretical lattice constant $a_0 = 5.4318 \text{ \AA}$ (216 Si atoms). Defect structures were optimized by minimization of the Hellmann-Feynman forces within the HSE06-level, until the largest force became lower than 0.01 eV/\AA . The band structure was sampled on a $2 \times 2 \times 2$ Monkhorst-Pack grid of **k**-points. Such sampling level leads to well converged formation energies, with a numerical accuracy of the order of 10 meV (see for example Ref. [93]).

Formation energies (E_{f}) and transition levels of defects (for instance with respect to the valence band top, $E(q/q') - E_{\text{v}}$) were evaluated using the usual respective methodologies [94],

$$E_{\text{f}}(q, E_{\text{F}}) = E_{\text{def}}(q) - \mu_{\text{ref}} + q(\varepsilon_{\text{v}} + E_{\text{F}})$$

and

$$E(q/q') - E_{\text{v}} = [E_{\text{def}}(q) - E_{\text{def}}(q')]/(q' - q) - \varepsilon_{\text{v}},$$

where $E_{\text{def}}(q)$ is the total energy of the defect in charge state q (which already includes a periodic charge correction [95]), μ_{ref} is a reference energy for a system with the same stoichiometry of the defective supercell, and the term $q(\varepsilon_{\text{v}} + E_{\text{F}})$ accounts for $-q$ electrons (or q holes) trapped at the defect. Finally, ε_{v} is the highest occupied state of bulk Si at **k** = Γ and E_{F} is the Fermi energy (independent variable).

For the calculation of μ_{ref} , energies of Si, H, B, Ga, P and C species were found from the energies per atom in bulk Si, molecular H_2 in Si, substitutional B, Ga, P and C in Si. For instance, the energy per substitutional species X was found from $\mu_X = E(\text{Si}_{215}X) - 215\mu_{\text{Si}}$, where $E(\text{Si}_{215}X)$ is the energy of a 216 atom cell where one of the Si atoms is replaced by X , and μ_{Si} is the energy per Si atom in bulk Si (silicon chemical potential).

The comparison of calculated transition levels of defects in semiconductors with experimental data, notably with levels measured by deep level transient spectroscopy [96, 97], is not always straightforward. The calculations are usually carried out at $T = 0$ K (like we did), they assume that the T -dependence of the energy of both charge states is identical, and that they benefit from cancellation effects. This condition is however not warranted, and as pointed out by Wickramaratne *et al.* [98], temperature dependencies of the carrier capture cross section might induce a gentle *bowing* to the Arrhenius-like plot of the T^2 -corrected emission rate against $1/k_{\text{B}}T$. This effect was estimated to lead to variations in the extracted activation energy of the order of ~ 0.1 eV across a temperature window of hundreds of Kelvin. For defects with emission peaks around ~ 100 K, such finite-temperature effects become smaller and the measured activation energies for carrier emission are closer to the 0 K extrapolation. The bowing is normally unnoticed simply because the range of temperatures that are allowed by the measurement conditions is limited.

Another effect to consider is the existence of a capture barrier. If the experiment involves the measurement of emission rates only, a capture barrier must be subtracted from the emission activation energy in order to find a level position [96, 97]. This barrier is also temperature dependent, it is usually small ($\lesssim 0.1$ eV) for defects with similar geometries in both charge states of the transition, and decreases substantially at cryogenic temperatures (below ~ 100 K) due to tunneling effects [79]. This effect should always be considered with care, especially when dealing with transitions involving a change in the defect structure. Many defects in Si have levels in the range of up to ~ 0.4 eV from the band edges, and temperature effects during the measurements are not as severe as in wide gap materials, where emission peaks are observed at few hundred Kelvin. Of course, calculating the temperature dependent capture cross section [78–80], and casting it in the form of an Arrhenius relation [98], would bring the calculations closer to what is actually measured. However, as referred at the end of Sec. III, we leave this task for future work.

Temperature-dependent free energies of defects were also estimated within several limitations, including the harmonic and dilute approximations, where anharmonicity and defect-defect interactions are neglected. In these calculations we account for the electronic potential energy, zero-point motion, as well as vibrational, rotational and configurational degrees of freedom. Further details have been reported elsewhere [24].

The potential energy landscape of reactions was investigated using the nudged elastic band (NEB) method [99]. Firstly, up to 12 intermediate geometries, all connected by the *elastic band* between the HSE06-level end-state geometries,

were relaxed. These calculations were performed within the generalized gradient approximation [100]. Secondly, single-point calculations at HSE06-level were performed for all geometries along the chain. From here, we found the minimum energy path (MEP) for the reaction of interest.

The above methodology relies on transition-state-theory, where the reactants are assumed to convert into the products once the saddle point – the highest energy state along the minimum energy path between the ends of the reaction – is achieved, the charge and magnetic state of the system is conserved along the way, and electron phonon coupling is neglected. Experimental conditions and limitations also hinder a direct comparison between measured and calculated figures. Important effects include back-reactions, interactions with intrinsic carriers, among other effects, which can only be acknowledged in the analysis, or roughly accounted for.

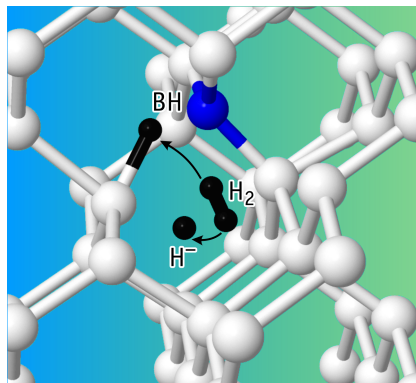
CONFLICT OF INTEREST

The authors declare no conflict of interest.

DATA AVAILABILITY STATEMENT

The data that support the findings of this study are available at request from the corresponding author.

TABLE OF CONTENTS



Caption of ToC figure: The thermodynamics of several reactions involving atomic and molecular hydrogen with group-III acceptors in silicon has been investigated theoretically. The results offer a first-principles-level account of thermally- and carrier-activated processes relevant to Light and elevated Temperature Induced Degradation (LeTID) of Si-based solar cells.

ACKNOWLEDGMENTS

We acknowledge the FCT through projects LA/P/0037/2020, UIDB/50025/2020, UIDP/50025/2020

and 2021.09643.CPCA (Advanced Computing Project using

the Oblivion supercomputer). The work in the UK was funded by EPSRC via grant EP/TO25131/1.

-
- [1] J. Schmidt and K. Bothe, *Physical Review B* **69**, 024107 (2004).
- [2] J. Lindroos and H. Savin, *Solar Energy Materials and Solar Cells* **147**, 115 (2016).
- [3] T. Niewelt, J. Schon, W. Warta, S. W. Glunz, and M. C. Schubert, *IEEE Journal of Photovoltaics* **7**, 383 (2017).
- [4] J. D. Murphy, A. I. Pointon, N. E. Grant, V. A. Shah, M. Myronov, V. V. Voronkov, and R. J. Falster, *Progress in Photovoltaics: Research and Applications* **27**, 844 (2019).
- [5] R. Chen, M. Wright, D. Chen, J. Yang, P. Zheng, X. Zhang, S. Wenham, and A. Ciesla, *Progress in Photovoltaics: Research and Applications* **29**, 1213 (2021).
- [6] C. Möller and K. Lauer, *physica status solidi (RRL) - Rapid Research Letters* **7**, 461 (2013).
- [7] E. Cho, Y.-W. Ok, A. D. Upadhyaya, M. J. Binns, J. Appel, J. Guo, and A. Rohatgi, *IEEE Journal of Photovoltaics* **6**, 795 (2016).
- [8] T. O. A. Fattah, V. P. Markevich, J. A. D. Guzman, J. Coutinho, N. V. Abrosimov, J. Binns, I. Crowe, M. P. Halsall, and A. R. Peaker, *SiliconPV 2022, The 12th International Conference on Crystalline Silicon Photovoltaics, AIP Conference Proceedings* **2826**, 110001 (2023).
- [9] *International Technology Roadmap for Photovoltaic (ITRPV), 2022 Results*, 14th ed. (VDMA, 2023).
- [10] K. Ramspeck, S. Zimmermann, H. Nagel, A. Metz, Y. Gassenbauer, B. Birkmann, and A. Seidl, in *Proceedings of the 27th European Photovoltaic Solar Energy Conference and Exhibition (WIP, 2012)* pp. 861–865.
- [11] D. Bredemeier, D. C. Walter, R. Heller, and J. Schmidt, *physica status solidi (RRL) – Rapid Research Letters* **13**, 1900201 (2019).
- [12] D. Chen, M. Kim, B. V. Stefani, B. J. Hallam, M. D. Abbott, C. E. Chan, R. Chen, D. N. R. Payne, N. Nampalli, A. Ciesla, T. H. Fung, K. Kim, and S. R. Wenham, *Solar Energy Materials and Solar Cells* **172**, 293 (2017).
- [13] D. Chen, P. G. Hamer, M. Kim, T. H. Fung, G. Bourret-Sicotte, S. Liu, C. E. Chan, A. Ciesla, R. Chen, M. D. Abbott, B. J. Hallam, and S. R. Wenham, *Solar Energy Materials and Solar Cells* **185**, 174 (2018).
- [14] D. Lin, Z. Hu, L. Song, D. Yang, and X. Yu, *Solar Energy* **225**, 407 (2021).
- [15] N. E. Grant, P. P. Altermatt, T. Niewelt, R. Post, W. Kwapil, M. C. Schubert, and J. D. Murphy, *Solar RRL* **5**, 2000754 (2021).
- [16] D. Chen, M. V. Contreras, A. Ciesla, P. Hamer, B. Hallam, M. Abbott, and C. Chan, *Progress in Photovoltaics: Research and Applications* **29**, 1180 (2020).
- [17] D. Chen, P. Hamer, M. Kim, C. Chan, A. C. nee Wenham, F. Rougieux, Y. Zhang, M. Abbott, and B. Hallam, *Solar Energy Materials and Solar Cells* **207**, 110353 (2020).
- [18] R. E. Pritchard, M. J. Ashwin, J. H. Tucker, and R. C. Newman, *Physical Review B* **57**, R15048 (1998).
- [19] R. E. Pritchard, J. H. Tucker, R. C. Newman, and E. C. Lightowers, *Semiconductor Science and Technology* **14**, 77 (1999).
- [20] M. Stavola, E. E. Chen, W. B. Fowler, and G. A. Shi, *Physica B: Condensed Matter* **340-342**, 58 (2003).
- [21] M. Sheoran, D. S. Kim, A. Rohatgi, H. F. W. Dekkers, G. Beaucarne, M. Young, and S. Asher, *Applied Physics Letters* **92**, 172107 (2008).
- [22] V. P. Markevich and M. Suezawa, *Journal of Applied Physics* **83**, 2988 (1998).
- [23] J. A. T. De Guzman, V. P. Markevich, J. Coutinho, N. V. Abrosimov, M. P. Halsall, and A. R. Peaker, *Solar RRL* **6**, 2100459 (2021).
- [24] J. Coutinho, D. Gomes, V. J. B. Torres, T. O. A. Fattah, V. P. Markevich, and A. R. Peaker, *Physical Review B* **108**, 014111 (2023).
- [25] D. Gomes, V. P. Markevich, A. R. Peaker, and J. Coutinho, *physica status solidi (b)* **259**, 2100670 (2022).
- [26] C. Vargas, G. Coletti, C. Chan, D. Payne, and Z. Hameiri, *Solar Energy Materials and Solar Cells* **189**, 166 (2019).
- [27] B. Hammann, L. Rachdi, W. Kwapil, F. Schindler, and M. C. Schubert, *physica status solidi (RRL) – Rapid Research Letters* **15**, 2000584 (2021).
- [28] B. Hammann, N. Assmann, P. M. Weiser, W. Kwapil, T. Niewelt, F. Schindler, R. Sondena, E. V. Monakhov, and M. C. Schubert, *IEEE Journal of Photovoltaics* **13**, 224 (2023).
- [29] T. O. A. Fattah, V. P. Markevich, D. Gomes, J. Coutinho, N. V. Abrosimov, I. D. Hawkins, M. P. Halsall, and A. R. Peaker, *to appear in Solar Energy Materials and Solar Cells* **259**, 112447 (2023).
- [30] W. Kwapil, J. Dalke, R. Post, and T. Niewelt, *Solar RRL* , 2100147 (2021).
- [31] R. Post, T. Niewelt, W. Kwapil, and M. Schubert, *IEEE Journal of Photovoltaics* **12**, 238 (2022).
- [32] D. Kang, H. C. Sio, X. Zhang, Q. Wang, H. Jin, and D. Macdonald, in *Proceedings of the 36th European Photovoltaic Solar Energy Conference and Exhibition (WIP, 2019)* pp. 318–321.
- [33] M. A. Green, *Solar Energy Materials and Solar Cells* **143**, 190 (2015).
- [34] N. Nickel, ed., *Hydrogen in Semiconductors II*, Semiconductors and semimetals, Vol. 61 (Academic Press, San Diego, 1999).
- [35] S. K. Estreicher, M. Stavola, and J. Weber, *Silicon, germanium, and their alloys* (CRC Press, Boca Raton, 2015) Chap. 7, pp. 217–254.
- [36] K. B. Nielsen, B. B. Nielsen, J. Hansen, E. Andersen, and J. U. Andersen, *Physical Review B* **60**, 1716 (1999).
- [37] C. Herring, N. M. Johnson, and C. G. Van de Walle, *Physical Review B* **64**, 125209 (2001).
- [38] K. B. Nielsen, L. Dobaczewski, S. Søgård, and B. B. Nielsen, *Physical Review B* **65**, 075205 (2002).
- [39] P. Deák, L. C. Snyder, and J. W. Corbett, *Physical Review B* **37**, 6887 (1988).
- [40] C. G. V. de Walle, P. J. H. Denteneer, Y. Bar-Yam, and S. T. Pantelides, *Physical Review B* **39**, 10791 (1989).
- [41] N. M. Johnson, C. Herring, and C. G. Van de Walle, *Physical Review Letters* **73**, 130 (1994).
- [42] C. Sun, A. Liu, S. P. Phang, F. E. Rougieux, and D. Macdonald, *Journal of Applied Physics* **118**, 10.1063/1.4929757 (2015).
- [43] C. Sun, D. Yan, and D. Macdonald, *physica status solidi*

- (RRL) – Rapid Research Letters **15**, 2100483 (2021).
- [44] Y. V. Gorelkinskii and N. N. Nevinnyi, *Materials Science and Engineering: B* **36**, 133 (1996).
- [45] C. Langpape, S. Fabian, C. Klatt, and S. Kalbitzer, *Applied Physics A: Materials Science & Processing* **64**, 207 (1997).
- [46] N. M. Johnson, C. Herring, and D. J. Chadi, *Physical Review Letters* **56**, 769 (1986).
- [47] K. Bergman, M. Stavola, S. J. Pearton, and J. Lopata, *Physical Review B* **37**, 2770 (1988).
- [48] K. J. Chang and D. J. Chadi, *Physical Review Letters* **60**, 1422 (1988).
- [49] S. K. Estreicher, L. Throckmorton, and D. S. Marynick, *Physical Review B* **103**, 13241 (1998).
- [50] J. Zhu, N. M. Johnson, and C. Herring, *Physical Review B* **41**, 12354 (1990).
- [51] A. J. Tavendale, S. J. Pearton, and A. A. Williams, *Applied Physics Letters* **56**, 949 (1990).
- [52] N. Fukata, S. Sato, S. Fukuda, K. Ishioka, M. Kitajima, S. Hishita, and K. Murakami, *Physica B: Condensed Matter* **401-402**, 175 (2007).
- [53] P. J. H. Denteneer, C. G. V. de Walle, and S. T. Pantelides, *Physical Review B* **41**, 3885 (1990).
- [54] S. J. Pearton and J. Lopata, *Applied Physics Letters* **59**, 2841 (1991).
- [55] C. H. Seager and R. A. Anderson, *Solid State Communications* **76**, 285 (1990).
- [56] N. M. Johnson and C. Herring, *Physical Review B* **45**, 11379 (1992).
- [57] C. H. Seager and R. A. Anderson, *Applied Physics Letters* **63**, 1531 (1993).
- [58] N. M. Johnson and C. Herring, *Physical Review B* **46**, 15554 (1992).
- [59] S. K. Estreicher, C. H. Seager, and R. A. Anderson, *Applied Physics Letters* **59**, 1773 (1991).
- [60] S. K. Estreicher and R. Jones, *Applied Physics Letters* **64**, 1670 (1994).
- [61] S. K. Estreicher, *Physical Review B* **41**, 9886 (1990).
- [62] B. B. Nielsen, K. Tanderup, M. Budde, K. B. Nielsen, J. L. Lindström, R. Jones, S. Öberg, B. Hourahine, and P. R. Briddon, *Materials Science Forum* **258-263**, 391 (1997).
- [63] M. Ramamoorthy and S. T. Pantelides, *Solid State Communications* **106**, 243 (1998).
- [64] R. B. Capaz, L. V. C. Assali, L. C. Kimerling, K. Cho, and J. D. Joannopoulos, *Physical Review B* **59**, 4898 (1999).
- [65] M. Suezawa, *Japanese Journal of Applied Physics* **38**, L484 (1999).
- [66] V. P. Markevich, L. I. Murin, J. Hermansson, M. Kleverman, J. L. Lindström, N. Fukata, and M. Suezawa, *Physica B: Condensed Matter* **302-303**, 220 (2001).
- [67] B. Hourahine, R. Jones, S. Öberg, P. R. Briddon, V. P. Markevich, R. C. Newman, J. Hermansson, M. Kleverman, J. L. Lindström, L. I. Murin, N. Fukata, and M. Suezawa, *Physica B: Condensed Matter* **308-310**, 197 (2001).
- [68] S. K. Estreicher, A. Docaj, M. B. Bebek, D. J. Backlund, and M. Stavola, *physica status solidi (a)* **209**, 1872 (2012).
- [69] O. Andersen, A. R. Peaker, L. Dobaczewski, K. B. Nielsen, B. Hourahine, R. Jones, P. R. Briddon, and S. Öberg, *Physical Review B* **66**, 235205 (2002).
- [70] Y. K. Y. Kamiura, M. H. M. Hayashi, Y. N. Y. Nishiyama, S. O. S. Ohyama, and Y. Y. Y. Yamashita, *Japanese Journal of Applied Physics* **36**, 6579 (1997).
- [71] Y. Kamiura, M. Tsutsue, Y. Yamashita, F. Hashimoto, and K. Okuno, *Journal of Applied Physics* **78**, 4478 (1995).
- [72] V. Kolkovsky, R. Stübner, K. Gwozdz, and J. Weber, *Physica B: Condensed Matter* **535**, 128 (2018).
- [73] T. Zundel and J. Weber, *Physical Review B* **39**, 13549 (1989).
- [74] K. J. Chang and D. J. Chadi, *Physical Review B* **40**, 11644 (1989).
- [75] S. K. Estreicher, M. Sanati, D. West, and F. Ruymgaart, *Physical Review B* **70**, 125209 (2004).
- [76] A. B. Sproul and M. A. Green, *Journal of Applied Physics* **70**, 846 (1991).
- [77] C. H. Seager and R. A. Anderson, *Applied Physics Letters* **59**, 585 (1991).
- [78] L. Shi and L.-W. Wang, *Physical Review Letters* **109**, 245501 (2012).
- [79] A. Alkauskas, Q. Yan, and C. G. V. de Walle, *Physical Review B* **90**, 075202 (2014).
- [80] S. Kim, S. N. Hood, and A. Walsh, *Physical Review B* **100**, 041202 (2019).
- [81] P. Leary, R. Jones, and S. Öberg, *Physical Review B* **57**, 3887 (1998).
- [82] R. Stübner, V. Kolkovsky, L. Scheffler, and J. Weber, *physica status solidi c* **13**, 770 (2016).
- [83] J. Coutinho, O. Andersen, L. Dobaczewski, K. B. Nielsen, A. R. Peaker, R. Jones, S. Öberg, and P. R. Briddon, *Physical Review B* **68**, 184106 (2003).
- [84] R. Stübner, L. Scheffler, V. Kolkovsky, and J. Weber, *Journal of Applied Physics* **119**, 10.1063/1.4952702 (2016).
- [85] J. D. Holbeck, B. B. Nielsen, R. Jones, P. Sitch, and S. Öberg, *Physical Review Letters* **71**, 875 (1993).
- [86] S. K. Estreicher, J. L. Hastings, and P. A. Fedders, *Physical Review Letters* **82**, 815 (1999).
- [87] G. Kresse and J. Hafner, *Physical Review B* **47**, 558 (1993).
- [88] G. Kresse and J. Furthmüller, *Computational Materials Science* **6**, 15 (1996).
- [89] G. Kresse and J. Furthmüller, *Physical Review B* **54**, 11169 (1996).
- [90] P. E. Blöchl, *Physical Review B* **50**, 17953 (1994).
- [91] J. Heyd, G. E. Scuseria, and M. Ernzerhof, *The Journal of Chemical Physics* **118**, 8207 (2003).
- [92] A. V. Krukau, O. A. Vydrov, A. F. Izmaylov, and G. E. Scuseria, *The Journal of Chemical Physics* **125**, 10.1063/1.2404663 (2006).
- [93] J. Shim, E.-K. Lee, Y. J. Lee, and R. M. Nieminen, *Physical Review B* **71**, 245204 (2005).
- [94] C. Freysoldt, B. Grabowski, T. Hickel, J. Neugebauer, G. Kresse, A. Janotti, and C. G. V. de Walle, *Reviews of Modern Physics* **86**, 253 (2014).
- [95] C. Freysoldt, J. Neugebauer, and C. G. Van de Walle, *Physical Review Letters* **102**, 016402 (2009).
- [96] C. H. Henry and D. V. Lang, *Physical Review B* **15**, 989 (1977).
- [97] A. R. Peaker, V. P. Markevich, and J. Coutinho, *Journal of Applied Physics* **123**, 161559 (2018).
- [98] D. Wickramaratne, C. E. Dreyer, B. Monserrat, J.-X. Shen, J. L. Lyons, A. Alkauskas, and C. G. V. de Walle, *Applied Physics Letters* **113**, 192106 (2018).
- [99] G. Henkelman, B. P. Uberuaga, and H. Jónsson, *The Journal of Chemical Physics* **113**, 9901 (2000).
- [100] J. P. Perdew, K. Burke, and M. Ernzerhof, *Physical Review Letters* **77**, 3865 (1996).

Supporting Information: Hydrogen reactions with dopants and impurities in solar silicon from first principles

José Coutinho, Diana Gomes, and Vitor J. B. Torres
*i3N and Department of Physics, University of Aveiro, Campus Santiago, 3810-193 Aveiro, Portugal**

Tarek O. Abdul Fattah, Vladimir P. Markevich, and Anthony R. Peaker
*Photon Science Institute and Department of Electrical and Electronic Engineering,
 The University of Manchester, Manchester M13 9PL, United Kingdom*

Published with Solar RRL 8, 2300639 (2024)

DOI: [10.1002/solr.202300639](https://doi.org/10.1002/solr.202300639)

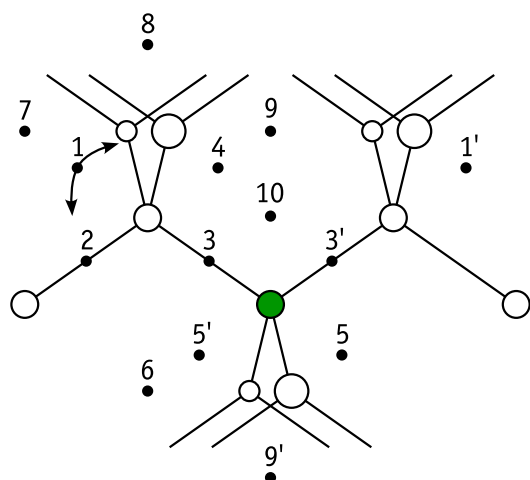


Figure S1. Schematic geometries of the different PH pairs that were investigated. The position of the H atom is indicated by a small dot along with an index. Primed and non-primed indexes are equivalent by symmetry. P and Si atoms are shown in green and white, respectively. These correspond to approximate positions in the initial geometries (before atomic relaxation). Structures that were not stable and “collapsed” to a lower energy configuration upon energy minimization are indicated Table S1 below. The two-way arrow indicates the wagging mode of H discussed in the context of the light/injection enhanced dissociation of PH.

Table S1. Calculated relative energies of PH pairs with respect to the lowest energy configuration (zero energy). The structure index (first column) corresponds to the location of H as indicated in Figure S1 above. Some structures have a PH_X label as used in the article. For some structures, $\rightarrow i$ indicates that they are unstable in that specific charge state, and relax to another structure with index i during force and energy minimization. Configurations without energy did not possess gap states capable of trapping holes. No acceptor (negatively charged) states were found. All values are in eV.

Index	Label	$E_{\text{rel}}(q=0)$	$E_{\text{rel}}(q=+1)$	$E_{\text{rel}}(q=+2)$
1	PH_{AB}	0.00		
2	PH_{BC1}	1.14	0.14	0.31
3	PH_{BC}	0.45	0.00	
4		0.35	0.20	
5		0.53	0.31	
6		0.61	0.38	
7		$\rightarrow 1$	0.27	
8		0.70	0.29	
9		0.39	0.37	
10		$\rightarrow 4$	$\rightarrow 3$	
11	$\text{P} + \text{H}_{\text{BC}}$	1.36	0.14	0.00

* jose.coutinho@ua.pt

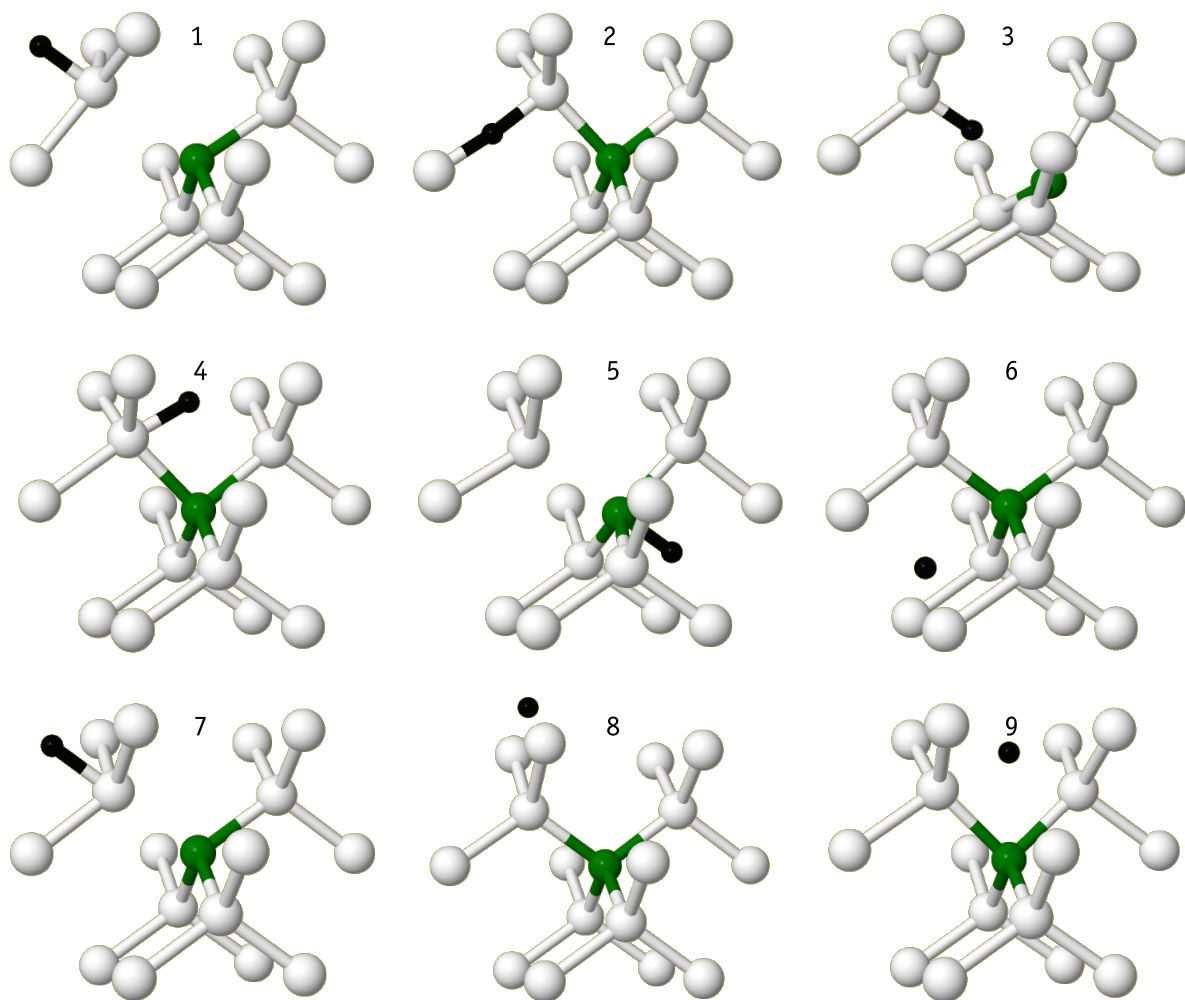


Figure S2. Atomistic geometries of several PH pairs after relaxation. P, Si and H atoms are shown in green, white, and black respectively. All structures but number 7 (which is positively charged) correspond to the neutral charge state. Relative energies are indicated in Table S1.